Aerodynamic Shape Optimization with Uncertain Operating Conditions using Metamodels

Régis Duvigneau

INRIA

INSTITUT NATIONAL DE RECHERCHE EN INFORMATIQUE ET EN AUTOMATIQUE

Aerodynamic Shape Optimization with Uncertain Operating Conditions using Metamodels

Régis Duvigneau

N° 6143

Mars 2007

Thème NUM

ISSN 0249-6399 ISRN INRIA/RR--6143--FR+ENG

INRIA
SOPHIA ANTIPOLIS

Aerodynamic Shape Optimization with Uncertain Operating Conditions using Metamodels

Régis Duvigneau*

Thème NUM — Systèmes numériques
Projet Opale

Rapport de recherche n° 6143 — Mars 2007 — 32 pages

Abstract: In this paper, we address aerodynamic shape optimization problems including uncertain operating conditions. After a review of the possible approaches to take into account uncertainty, we propose to use meta-modeling techniques in order to develop a two-level modeling procedure for statistics estimation. Radial basis functions are employed to approximate the aerodynamic coefficients as operating conditions vary. Then, a Monte-Carlo method is employed to estimate statistics using the approximate model. The proposed approach is applied to the robust optimization of the wing shape of a business aircraft, by minimizing the mean and the variance of the drag coefficient with uncertain free-stream Mach number.

Key-words: Shape optimization, Uncertainty, Robust design, Metamodels, Aerodynamics.

* Opale Project-Team

Unité de recherche INRIA Sophia Antipolis
2004, route des Lucioles, BP 93, 06902 Sophia Antipolis Cedex (France)
Téléphone : +33 4 92 38 77 77 — Télécopie : +33 4 92 38 77 65

Optimisation de forme aérodynamique avec conditions de fonctionnement incertaines utilisant des métamodèles

Résumé : On aborde dans ce rapport des problèmes d'optimisation de forme aérodynamique incluant des conditions de fonctionnement incertaines. Après un bilan des approches possibles pour prendre en compte les incertitudes, on propose d'utiliser des méta-modèles pour développer une procédure à deux niveaux de modélisation pour l'estimation de statistiques. Des fonctions à base radiale sont utilisées pour approcher les coefficients aérodynamiques lorsque les conditions de fonctionnement varient. Ensuite, une méthode de Monte-Carlo est employée pour estimer des statistiques en utilisant le modèle approché. La méthode proposée est appliquée à l'optimisation robuste de l'aile d'un avion d'affaire, en minimisant la moyenne et la variance du coefficient de traînée avec un nombre de Mach amont uncertain.

Mots-clés : Optimisation de forme, incertitudes, conception robuste, métamodèles, aérodynamique.

Contents

1 Introduction to robust design **5**
1.1 Deterministic shape optimization problem . . . 5
1.2 Motivation for optimization under uncertainty . . . 5
1.3 Methods for robust design . . . 6
1.3.1 Multipoint approach . . . 6
1.3.2 Worst-case approach . . . 6
1.3.3 Interval analysis approach . . . 7
1.3.4 Statistical approach . . . 8

2 Statistical approach for robust design **9**
2.1 Uncertainty estimation . . . 9
2.1.1 Deterministic viewpoint . . . 9
2.1.2 Stochastic viewpoint . . . 9
2.2 Cost function approximation . . . 10
2.2.1 Taylor series approximation . . . 10
2.2.2 Radial Basis Functions . . . 11
2.3 Robust optimization problem . . . 12

3 Application to wing design with uncertain Mach number **13**
3.1 Problem description . . . 13
3.1.1 Testcase . . . 13
3.1.2 Parameterization . . . 14
3.1.3 Aerodynamic analysis . . . 15
3.1.4 Optimization algorithm . . . 16
3.2 Single-point optimization . . . 18
3.3 Study of uncertainty propagation . . . 22
3.4 Results for robust design . . . 25
3.4.1 Pareto front . . . 25
3.4.2 Drag coefficient variations . . . 25
3.4.3 A posteriori validation . . . 26
3.4.4 Shape comparison . . . 27
3.4.5 Flow analysis . . . 27

Introduction

Thanks to the recent improvements of numerical methods in Computational Fluid Dynamics (CFD) and the developement of high performance computing capabilities, complex and realistic problems for industrial applications are now addressed by engineers using numerical simulation. In this context, the study of the sources of uncertainty and error in CFD results has been an increasing research topic for the last years.

Before discussing of uncertainty and error sources and their classification, their definition is reminded: according to AIAA (American Institute of Aeronautics ans Astronautics), the uncertainty in CFD is "a potential deficiency in any phase or activity of the modeling process that is due to lack of knowledge" [1]. This definition underlines the stochastic nature of uncertainty. On the contrary, error in CFD simulations is clearly deterministic and is defined as "a recognizable deficiency in any phase or activity of the modeling process that is not due to lack of knowledge" [1]. These two concepts sometimes lead to confusion.

In [35], sources of uncertainty and error are analysed and classified into four main categories:

1. Physical modeling:
   (a) Assumptions in the PDE: inviscid flow, viscous flow, incompressible flow, chemically reacting gas, transitional or turbulent flow, etc ;
   (b) Auxiliary models: state equation, thermodynamic properties, tranports properties, chemical models, reaction and rates, turbulence model, etc ;
   (c) Boundary conditions : wall roughness, far field conditions, free-surface conditions, geometry description, etc ;
2. Discretization and solution : truncation error (spatial and temporal), iterative convergence, discrete geometry representation, etc ;
3. Round-off error: finite precision arithmetic ;
4. Programming and user error ;

The analysis and quantification of uncertainty and error due to these different sources have been studied by several authors. Particularly, discretization error has been studied in [38]. Grid adaption techniques (see for instance [9, 22, 25, 44]) have been proposed to control this error. The influence of geometrical uncertainty has been addressed in [13, 20], whereas uncertainty related to turbulence modeling has been studied in [21, 41, 42]. The influence of uncertain physical parameters for boundary conditions has been adressed in [23].

Some sources of error can be made negligible thanks to the increase of computational resources, such as discretization error, iterative convergence error, etc. However, other sources of error or uncertainty remain significant and motivate further research in this field.

This paper deals with uncertainty analysis related to fluctuating operating conditions. We are interested in quantifying the influence of this uncertainty on aerodynamic performance for shape optimization purpose. The final goal of this study is to propose an algorithm to take into account this uncertainty into an automatic shape optimization procedure.

In the first part of the paper, the optimization problem under uncertainty is defined and a review of the possible approaches to take into account uncertainty in the design procedure is achieved.

In a second part, we propose a method that relies on meta-models to estimate statistics in a two-level modeling procedure.

In a third part, the proposed method is demonstrated by optimizing a wing shape of a business aircraft with uncertain free-stream Mach number. The objective of the problem is to reduce both the mean and the variance of the drag coefficient.

1 Introduction to robust design

1.1 Deterministic shape optimization problem

A deterministic simulation-based shape optimization problem consists in minimizing a cost function $\mathcal{J}$, which depends on a shape Γ and state variables W. In parametric approaches, the shape Γ is represented by a small number of design variables $\mathbf{x} = (x^i)_{i=1,\dots,n}$, which are considered as optimization variables. The use of such a parametric approach allows to replace the initial shape optimization problem of infinite dimension by a problem with a finite number n of unknowns. State variables W (i.e. physical flow fields) depend implicitly on the design variables through the state equations $\mathcal{E}(\mathbf{x}, W(\mathbf{x}, \mathbf{a})) = 0$, where $\mathbf{a} = (a^m)_{m=1,\dots,M}$ represents some parameters which define operating conditions such as Mach number, angle of attack, etc. Finally, a general parametric shape optimization problem can be expressed as :

$$\begin{aligned} &\text{Minimize } \mathcal{J}(\mathbf{x}, W(\mathbf{x}, \mathbf{a})) \quad \mathbf{x} \in \Re^n, \\ &\text{Subject to } \mathcal{C}(\mathbf{x}, W(\mathbf{x}, \mathbf{a})) \leq 0, \end{aligned} \tag{1}$$

where $\mathcal{C}$ represents additional (physical or geometrical) constraints. Several optimization strategies and numerical methods can be carried out to solve such a problem. Nevertheless, a typical algorithm to solve such a problem can be described as follows:

1. choose initial design variables $\mathbf{x}^{(0)}$;
   $k \leftarrow 0$;
2. begin iteration k of the optimization loop ;
3. solve the state equations $\mathcal{E}(\mathbf{x}^{(k)}, W(\mathbf{x}^{(k)}, \mathbf{a})) = 0$ yielding the state variables $W(\mathbf{x}^{(k)}, \mathbf{a})$;
4. estimate the cost function $\mathcal{J}(\mathbf{x}^{(k)}, W(\mathbf{x}^{(k)}, \mathbf{a}))$ and possibly its gradient $\nabla\mathcal{J}(\mathbf{x}^{(k)}, W(\mathbf{x}^{(k)}, \mathbf{a}))$;
5. update the design variables to $\mathbf{x}^{(k+1)}$ according to the optimization algorithm ;
6. finish iteration k of the optimization loop ;
   if a stopping criterion is reached then STOP ;
   else $k \leftarrow k + 1$ GOTO step (2).

This deterministic optimization problem has been solved using gradient-based methods or evolutionnary approaches in various fields, such as aerodynamics [4, 5, 16, 26, 31, 34], hydrodynamics [7, 15], turbomachinery [10], thermodynamics [14], etc.

1.2 Motivation for optimization under uncertainty

Simulation-based design optimization in aerodynamics has been an active research topic for the last years and is now applied to industrial problems, as shown in previous references. For a long time, optimization exercises were carried out neglecting uncertainty. It is mainly due to the fact that CFD-based design methodologies were developed by CFD experts, who were not very familiar with uncertainty analysis and management.

However, application of such deterministic methods can lead to unexpected performance losses in practice and unacceptable results. Indeed, the prescribed optimized design is subject to inherent geometrical variations due to manufacturing tolerances. Moreover, operating conditions, such as Mach number, angle of attack, etc, are subject to variability and random fluctuations. Therefore, the fitness of the optimal design predicted by CFD is usually not obtained in practice, due to geometrical uncertainty and operating condition uncertainty.

To overcome this difficulty, robust and reliability-based design methods are developed, that assess the effects of uncertainty on the design performance during the optimization procedure. The objective of *robust design* methods is to minimize the performance loss due to everyday fluctuations, whereas the aim of *reliability-based design* methods is to manage the consequences of extreme events (see figure 1 from [23]). The present work is focused on the development of numerical methods for robust design in the framework of realistic aerodynamic problems. Moreover, we suppose in the next sections that uncertainty only originates from fluctuating operating conditions. Uncertainty due to geometrical tolerances is not addressed here.

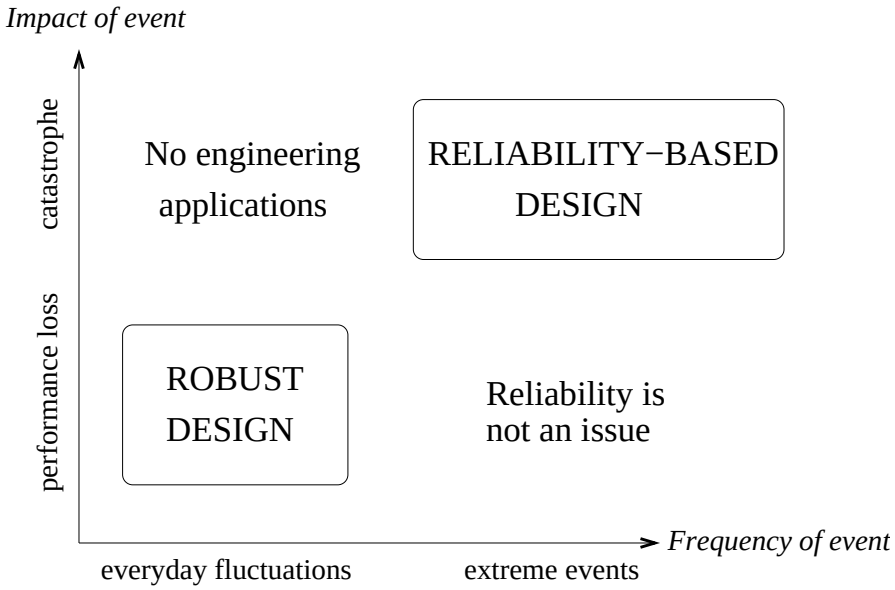

Figure 1: Optimization under uncertainty classification.

1.3 Methods for robust design

1.3.1 Multipoint approach

In aerodynamics, first attempts to reduce the sensitivity of the optimal design to operating conditions consisted in solving multipoint optimization problems, to prevent from a possibly severe degradation in the off-design performance. A multipoint optimization problem consists in replacing the cost function in the classical formulation (1), that is evaluated for a particular set of operating conditions $\mathbf{a}$, by a weighted sum of N cost functions evaluated at different sets of operating conditions $(\mathbf{a}_i)_{i=1,\dots,N}$:

$$\begin{aligned} &\text{Minimize } \sum_{i=1}^{N} \omega_i \mathcal{J}(\mathbf{x}, W(\mathbf{x}, \mathbf{a}_i)) \quad \mathbf{x} \in \Re^n \quad \sum_{i=1}^{N} \omega_i = 1, \\ &\text{Subject to } \mathcal{C}(\mathbf{x}, W(x, \mathbf{a}_i)) \leq 0 \quad i = 1, \dots, N. \end{aligned} \tag{2}$$

This strategy has been applied to airfoil design in order to reduce the drag over a Mach range or optimize the shape at cruise and landing flight conditions simultaneously (see for instance [17, 29, 33]). The main difficulty related to this approach is the well known "point-optimization effect": the solution depends critically on the choice of operating conditions $(\mathbf{a}_i)_{i=1,\dots,N}$. Since no requirement is imposed for the cost function at other operating conditions, the optimizer yield a design fully adapted to the N operating conditions under consideration $(\mathbf{a}_i)_{i=1,\dots,N}$, and the optimized design presents performance degradation for intermediate operating conditions. It was shown in [29] that in order to avoid the point-optimization effect, the number N of operating conditions should be larger than the number n of design variables. Therefore, this approach cannot be considered as a satisfactory answer to robust design problems.

Some improvements of the classical multipoint approach have been reported in [24] and [29]. In the former, a random choice of the operating conditions $(\mathbf{a}_i)_{i=1,\dots,N}$ in a given interval $[\mathbf{a}_{min}, \mathbf{a}_{max}]$ for each cost function evaluation was proposed to avoid the tedious choice of operating conditions. In the latter, a new scheme was proposed, called *profile optimization method*, that relies on adaptive adjustments of the weights $(\omega_i)_{i=1,\dots,N}$ to achieve a consistent reduction of the cost function $\mathcal{J}$ over a range of operating conditions. In [47] adaptive weigths is also proposed in conjunction with a new scheme that permits to automatically add new points to prevent from off-design loss.

1.3.2 Worst-case approach

This approach proposes to mitigate the detrimental effects of the worst-case performance. The objective of such a method is to determine a shape, whose worst performance for operating conditions varying in a given

interval, is as good as possible. Then, the aim is not to obtain a satisfactory fitness for random fluctuations of operating conditions, but to ensure that the performance degradation at the worst operating conditions is as small as possible.

For a given shape defined by $\mathbf{x}$, suppose that $\tilde{\mathbf{a}}(\mathbf{x})$ represents the operating conditions for which the cost function is the worst over a given range $[\mathbf{a}_{min}, \mathbf{a}_{max}]$:

$$\begin{array}{l} \text{Maximize } \mathcal{J}(\mathbf{x}, W(\mathbf{x}, \mathbf{a})) \quad \mathbf{a} \in [\mathbf{a}_{min}, \mathbf{a}_{max}], \\ \text{Subject to } \mathcal{C}(\mathbf{x}, W(\mathbf{x}, \mathbf{a})) \leq 0. \end{array} \tag{3}$$

The corresponding cost function value is:

$$\mathcal{J}_{max}(\mathbf{x}) = \mathcal{J}(\mathbf{x}, W(\mathbf{x}, \tilde{\mathbf{a}}(\mathbf{x}))). \tag{4}$$

Then, the shape optimization problem becomes:

$$\text{Minimize } \mathcal{J}_{max}(\mathbf{x}) \quad \mathbf{x} \in \Re^n. \tag{5}$$

This problem belongs to the class of well known "MinMax" problems, since for each step of the minimization problem (5), the maximization subproblem (3) has to be solved first. Due to the difficulty to solve such problems (that can be non-differentiable), a discrete formulation is often adopted in practice by replacing (3) by:

$$\begin{array}{l} \text{Maximize } \mathcal{J}(\mathbf{x}, W(\mathbf{x}, \mathbf{a}_i)) \quad i = 1, \ldots, N, \\ \text{Subject to } \mathcal{C}(\mathbf{x}, W(\mathbf{x}, \mathbf{a}_i)) \leq 0, \end{array} \tag{6}$$

where $(\mathbf{a}_i)_{i=1,\ldots,N}$ is a discretization of the interval $[\mathbf{a}_{min}, \mathbf{a}_{max}]$. Although this formulation seems different than the multipoint approach, it has been shown in the context of airfoil design (see [29]) that these problems can be mathematically equivalent under some assumptions. Therefore, the discrete approach (6) tends also to produce results that depend critically on the choice of operating conditions $(\mathbf{a}_i)_{i=1,\ldots,N}$. More generally, this approach only improves the worst-case performance and does not consider the global behavior of the fitness when operating conditions fluctuate.

1.3.3 Interval analysis approach

The basic idea of interval analysis is to determine the interval in which the cost function varies as the operating conditions fluctuate in a given interval. Then, a two-objective optimization problem is solved, that consists in minimizing the median value of the cost function, while minimizing the extent of its interval of variation.

Suppose that operating conditions fluctuate in the interval $[\mathbf{a}_{min}, \mathbf{a}_{max}]$. For a given shape defined by $\mathbf{x}$, the operating conditions $\hat{\mathbf{a}}(\mathbf{x})$ and $\tilde{\mathbf{a}}(\mathbf{x})$ that respectively correspond to the best and worst cost function values, are obtained by solving the two following subproblems:

$$\begin{array}{l} \text{Maximize } \mathcal{J}(\mathbf{x}, W(\mathbf{x}, \mathbf{a})) \quad \mathbf{a} \in [\mathbf{a}_{min}, \mathbf{a}_{max}], \\ \text{Subject to } \mathcal{C}(\mathbf{x}, W(\mathbf{x}, \mathbf{a})) \leq 0; \end{array} \tag{7}$$

$$\begin{array}{l} \text{Minimize } \mathcal{J}(\mathbf{x}, W(\mathbf{x}, \mathbf{a})) \quad \mathbf{a} \in [\mathbf{a}_{min}, \mathbf{a}_{max}], \\ \text{Subject to } \mathcal{C}(\mathbf{x}, W(\mathbf{x}, \mathbf{a})) \leq 0. \end{array} \tag{8}$$

The corresponding best and worst cost function values are:

$$\mathcal{J}_{min}(\mathbf{x}) = \mathcal{J}(\mathbf{x}, W(\mathbf{x}, \hat{\mathbf{a}}(\mathbf{x}))) \quad \mathcal{J}_{max}(\mathbf{x}) = \mathcal{J}(\mathbf{x}, W(\mathbf{x}, \tilde{\mathbf{a}}(\mathbf{x}))). \tag{9}$$

Then, the two-objective shape optimization problem is solved:

$$\text{Minimize } \left\{ \begin{array}{l} \left(\mathcal{J}_{max}(\mathbf{x}) + \mathcal{J}_{min}(\mathbf{x})\right)/2 \\ \left(\mathcal{J}_{max}(\mathbf{x}) - \mathcal{J}_{min}(\mathbf{x})\right) \end{array} \right. \quad x \in \Re^n. \tag{10}$$

Contrary to the previous methods, the interval analysis approach clearly defines robust design as a compromise between two goals: increase the fitness of the system and reduce the fitness variations. Despite this improvement, the method has several drawbacks. First, the two subproblems are similar to (3) for the worst-case approach. As explained above, solving directly this kind of problems is tedious for complex applications. Some softwares exist, that automatically perform interval analysis. However, as explained in [46], their use in the context of CFD solvers exhibits significant difficulties, due to the algorithmic complexity of such codes. Secondly, this approach does not take into account the fitness variations inside the interval $[\mathcal{J}_{min}(\mathbf{x}), \mathcal{J}_{max}(\mathbf{x})]$. Only extreme events are considered for the shape optimization problem (10).

1.3.4 Statistical approach

In the statistical approach, one considers the fluctuating operating conditions $\mathbf{a} = (a^m)_{m=1,\dots,M}$ as samples of random variables $\mathbf{A} = (A^m)_{m=1,\dots,M}$, whose statistical characteristics are known (mean $\boldsymbol{\mu}_\mathbf{A} = (\mu_A^m)_{m=1,\dots,M}$, variance $\boldsymbol{\sigma}^2_\mathbf{A} = ({\sigma_A^2}^m)_{m=1,\dots,M}$, etc). One also supposes for the sake of simplicity that the random variables $(A^m)_{m=1,\dots,M}$ are independent. The statistical characteristics of operating conditions can be determined by experimental measurements or engineering experience. Gaussian Probability Density Functions (PDFs) or truncated Gaussian PDFs are often used in practice (see [23] for instance).

The main consequence of this assumption is that the cost function of the problem is also a random variable J. According to the Von Neumann-Morgenstern decision theory [3, 23], the best choice is then to select the design which leads to the best expected fitness. This is known as the Maximum Expected Value (MEV) criterion. The decision or design that minimizes the risk is known as the "Bayes'decision" and is solution of the following problem:

$$\begin{aligned} &\text{Minimize } \mu_J = \int_{\Omega(\mathbf{A})} \mathcal{J}(\mathbf{x}, W(\mathbf{x},\mathbf{a}))\, \rho_\mathbf{A}(\mathbf{a})\, d\mathbf{a} \quad \mathbf{x} \in \Re^n, \\ &\text{Subject to } P[\mathcal{C}(\mathbf{x}, W(\mathbf{x},\mathbf{A})) \leq 0] \geq p. \end{aligned} \tag{11}$$

$\Omega(\mathbf{A})$ and $\rho_\mathbf{A}$ are the range and the PDF of the random variable $\mathbf{A}$. Then, the MEV criterion just consists in minimizing the statistical mean μ_J of the cost function. One can notice that the constraint is now expressed with a probabilistic formulation: the probability P that the constraint $\mathcal{C}(\mathbf{x}, W(\mathbf{x},\mathbf{A})) \leq 0$ is verified should be larger than a prescribed value p.

This approach is a significant improvement over previous methods. The robust design problem is now considered within a rigorous statistical framework. This allows to take into account the random fluctuations of the fitness in the optimization problem, but also to care about the frequency of occurence of the events, thanks to PDFs. Then, the most probable events have a larger influence in the decision than extreme and unlikely events.

However, problem (11) does not address the variability of the fitness. The mean value of the fitness is the only criterion that is considered in the "Bayes'decision". For engineering problems, one also would like to select a design for which the fitness is not subject to large variations as operating conditions fluctuate. Then, a second criterion is often joined to the MEV criterion, that relies on the minimization of the variance σ_J^2 of the fitness:

$$\begin{aligned} &\text{Minimize } \left\{ \begin{array}{l} \mu_J = \displaystyle\int_{\Omega(\mathbf{A})} \mathcal{J}(\mathbf{x}, W(\mathbf{x},\mathbf{a}))\, \rho_\mathbf{A}(\mathbf{a})\, d\mathbf{a} \\ \sigma_J^2 = \displaystyle\int_{\Omega(\mathbf{A})} (\mathcal{J}(\mathbf{x}, W(\mathbf{x},\mathbf{a})) - \mu_J)^2\, \rho_\mathbf{A}(\mathbf{a})\, d\mathbf{a} \end{array} \right. \quad \mathbf{x} \in \Re^n, \\ &\text{Subject to } P[\mathcal{C}(\mathbf{x}, W(\mathbf{x},\mathbf{A})) \leq 0] \geq p. \end{aligned} \tag{12}$$

This approach aims at determining a trade-off between the expected fitness and the expected fitness variation as operating conditions randomly fluctuate. Although this approach is satisfactory from theorical and practical viewpoints, its application is not straigthforward. Particularly, the estimation of the mean and variance can be tedious for complex CFD applications. This issue is detailled in the next sections.

2 Statistical approach for robust design

2.1 Uncertainty estimation

The statistical approach described above relies on the estimation of statistical quantities related to the random cost function J, such as the mean μ_J and the variance σ_J^2. One supposes that the characteristics of the random operating conditions $\mathbf{A}$ are exactly known, such as its PDF $\rho_{\mathbf{A}}$, its mean $\boldsymbol{\mu}_{\mathbf{A}}$ and its variance $\boldsymbol{\sigma}_{\mathbf{A}}^{\mathbf{2}}$.

The random variable J is an output of a complex numerical simulation tool, such as a CFD solver, whereas $\mathbf{A}$ is an input parameter. Therefore, the main issue is the estimation of output uncertainty according to the knowledge of input uncertainty, i.e. the propagation of uncertainty through the CFD solver.

This problem can be addressed [46] by either deterministic or stochastic viewpoints.

2.1.1 Deterministic viewpoint

For a given design determined by $\mathbf{x}$, the statistical mean μ_J and variance σ_J^2 are defined by:

$$\mu_J = \int_{\Omega(\mathbf{A})} \mathcal{J}(\mathbf{x}, W(\mathbf{x}, \mathbf{a}))\, \rho_{\mathbf{A}}(\mathbf{a})\, d\mathbf{a}, \tag{13}$$

$$\sigma_J^2 = \int_{\Omega(\mathbf{A})} (\mathcal{J}(\mathbf{x}, W(\mathbf{x}, \mathbf{a})) - \mu_J)^2\, \rho_{\mathbf{A}}(\mathbf{a})\, d\mathbf{a}. \tag{14}$$

These integrals cannot be analytically evaluated since no analytical formulation of $\mathcal{J}$ is available. To estimate them, one should either provide an analytical approximation of the cost function or discretize the integrals. The latter solution is quite similar to the multipoint approach, since the integrals become weighted sums of cost functions evaluated for some prescribed operating conditions. Then, the former approach using an approximation $\tilde{\mathcal{J}}$ is usually preferred:

$$\tilde{\mu}_J = \int_{\Omega(\mathbf{A})} \tilde{\mathcal{J}}(\mathbf{x}, \mathbf{a})\, \rho_{\mathbf{A}}(\mathbf{a})\, d\mathbf{a}, \tag{15}$$

$$\tilde{\sigma}_J^2 = \int_{\Omega(\mathbf{A})} (\tilde{\mathcal{J}}(\mathbf{x}, \mathbf{a}) - \mu_J)^2\, \rho_{\mathbf{A}}(\mathbf{a})\, d\mathbf{a}. \tag{16}$$

2.1.2 Stochastic viewpoint

To estimate the mean and variance of the random variable J, one can simply use statistical estimators in a classical Monte-Carlo approach. A sample of operating conditions $(\mathbf{a}_i)_{i=1,\dots,N}$ of size N is generated according to the PDF $\rho_{\mathbf{A}}$. Then, unbiased estimators of the mean and variance are:

$$\mathcal{M}_J = \frac{1}{N} \sum_{i=1}^{N} \mathcal{J}(\mathbf{x}, W(\mathbf{x}, \mathbf{a}_i)), \tag{17}$$

$$\mathcal{S}_J^2 = \frac{1}{N-1} \sum_{i=1}^{N} (\mathcal{J}(\mathbf{x}, W(\mathbf{x}, \mathbf{a}_i)) - \mathcal{M}_J)^2. \tag{18}$$

This approach does not suffer from "point-optimization effect" since the sample $(\mathbf{a}_i)_{i=1,\dots,N}$ is generated randomly according to the PDF $\rho_{\mathbf{A}}$. However, it is well known that this stochastic approach requires a large sample to provide an accurate estimation of the statistics. For CFD applications, a direct Monte-Carlo method is not conceivable presently. Nevertheless, a cheaper approximation $\tilde{\mathcal{J}}$ of the cost function can be used in a Monte-Carlo approach to estimate the mean and the variance, as suggested in [27]:

$$\tilde{\mathcal{M}}_J = \frac{1}{N} \sum_{i=1}^{N} \tilde{\mathcal{J}}(\mathbf{x}, \mathbf{a}_i), \tag{19}$$

$$\tilde{\mathcal{S}}_J^2 = \frac{1}{N-1} \sum_{i=1}^{N} (\tilde{\mathcal{J}}(\mathbf{x}, \mathbf{a}_i) - \tilde{\mathcal{M}}_J)^2. \tag{20}$$

2.2 Cost function approximation

Approximate the cost function is mandatory for robust design, as explained above, to integrate the cost function over the range of operating conditions or to estimate the statistical characteristics using a Monte-Carlo method. Two possibilities are examined in the next sections: Taylor Series (TS) or Radial Basis Functions (RBFs).

2.2.1 Taylor series approximation

The cost function can be approximated by linear TS $\tilde{\mathcal{J}}_L$ or quadratic TS $\tilde{\mathcal{J}}_Q$ in the vicinity of the expected operating conditions μ_A:

$$\tilde{\mathcal{J}}_L(\mathbf{x},\mathbf{a}) = \mathcal{J}(\mathbf{x},W(\mathbf{x},\boldsymbol{\mu}_\mathbf{A})) + \sum_{m=1}^{M} \frac{\partial}{\partial A^m}\mathcal{J}(\mathbf{x},W(\mathbf{x},\mathbf{A}))\Big|_{\boldsymbol{\mu}_\mathbf{A}} (a^m - \mu_A^m), \tag{21}$$

$$\begin{aligned}\tilde{\mathcal{J}}_Q(\mathbf{x},\mathbf{a}) = \mathcal{J}(\mathbf{x},W(\mathbf{x},\boldsymbol{\mu}_\mathbf{A}))+ &\sum_{m=1}^{M} \frac{\partial}{\partial A^m}\mathcal{J}(\mathbf{x},W(\mathbf{x},\mathbf{A}))\Big|_{\boldsymbol{\mu}_\mathbf{A}} (a^m - \mu_A^m) \\ &+ \frac{1}{2}\sum_{m=1}^{M}\sum_{l=1}^{L} \frac{\partial^2}{\partial A^m \partial A^l}\mathcal{J}(\mathbf{x},W(\mathbf{x},\mathbf{A}))\Big|_{\boldsymbol{\mu}_\mathbf{A}} (a^m - \mu_A^m)(a^l - \mu_A^l).\end{aligned} \tag{22}$$

The use of the linear approximation (21) of the cost function to estimate the integral (15) yields a First-Order (FO) approximation of the statistical mean. This approach is known as the First-Order First-Moment (FOFM) method:

$$(\tilde{\mu}_J)^{FO} = \mathcal{J}(\mathbf{x},W(\mathbf{x},\boldsymbol{\mu}_\mathbf{A})). \tag{23}$$

The use of the linear approximation (21) of the cost function to estimate the integral (16) provides a first-order approximation of the variance, yielding the First-Order Second-Moment (FOSM) method:

$$(\tilde{\sigma}_J^2)^{FO} = \sum_{m=1}^{M} \left(\frac{\partial}{\partial A^m}\mathcal{J}(\mathbf{x},W(\mathbf{x},\mathbf{A}))\Big|_{\boldsymbol{\mu}_\mathbf{A}} \right)^2 (\sigma_A^m)^2. \tag{24}$$

Alternatively, the use of the quadratic approximation (22) of the cost function yields a Second-Order (SO) approximation of the mean. The Second-Order First-Moment (SOFM) method reads:

$$(\tilde{\mu}_J)^{SO} = \mathcal{J}(\mathbf{x},W(\mathbf{x},\boldsymbol{\mu}_\mathbf{A})) + \frac{1}{2}\sum_{m=1}^{M} \frac{\partial^2}{\partial A^m \partial A^m}\mathcal{J}(\mathbf{x},W(\mathbf{x},\mathbf{A}))\Big|_{\boldsymbol{\mu}_\mathbf{A}} (\sigma_A^m)^2. \tag{25}$$

If the quadratic approximation (22) of the cost function is employed to estimate the variance, a far more complex formula is obtained, that requires the third and forth moments of $\mathbf{A}$. Then, the Second-Order Second-Moment (SOSM) method usually relies on the integration of (16) using the linear approximation (21) of the cost function and the second-order estimation of the mean (25), which yields:

$$\begin{aligned}(\tilde{\sigma}_J^2)^{SO} = &\sum_{m=1}^{M} \left(\frac{\partial}{\partial A^m}\mathcal{J}(\mathbf{x},W(\mathbf{x},\mathbf{A}))\Big|_{\boldsymbol{\mu}_\mathbf{A}} \right)^2 (\sigma_A^m)^2 + \\ &\frac{1}{4}\sum_{m=1}^{M}\sum_{l=1}^{L} \frac{\partial^2}{\partial A^m \partial A^m}\mathcal{J}(\mathbf{x},W(\mathbf{x},\mathbf{A}))\Big|_{\boldsymbol{\mu}_\mathbf{A}} \frac{\partial^2}{\partial A^l \partial A^l}\mathcal{J}(\mathbf{x},W(\mathbf{x},\mathbf{A}))\Big|_{\boldsymbol{\mu}_\mathbf{A}} (\sigma_A^m)^2\,(\sigma_A^l)^2.\end{aligned} \tag{26}$$

However, if one supposes that $\mathbf{A}$ is ruled by a Gaussian PDF, the quadratic approximation (22) can be easily employed in conjunction with the second-order estimation of the mean (25). Then, the SOSM method reads:

$$\begin{aligned}(\tilde{\sigma}_J^2)^{SO} = &\sum_{m=1}^{M} \left(\frac{\partial}{\partial A^m}\mathcal{J}(\mathbf{x},W(\mathbf{x},\mathbf{A}))\Big|_{\boldsymbol{\mu}_\mathbf{A}} \right)^2 (\sigma_A^m)^2 + \\ &\frac{1}{2}\sum_{m=1}^{M}\sum_{l=1}^{L} \left(\frac{\partial^2}{\partial A^m \partial A^l}\mathcal{J}(\mathbf{x},W(\mathbf{x},\mathbf{A}))\Big|_{\boldsymbol{\mu}_\mathbf{A}} \right)^2 (\sigma_A^m)^2\,(\sigma_A^l)^2.\end{aligned} \tag{27}$$

As can be seen, for the FOFM method (23), the mean of the cost function is simply the cost function evaluated at the mean value of operating conditions. This assumption is only true for linear systems. In the SOFM method (25), a correction term is added that uses the second derivatives of the cost function. Note that the first derivatives have no influence on the mean value of the cost function. The estimation of the variance requires the first derivatives in the FOSM method (24) and the second derivatives in the SOSM method (26-27).

A polynomial approximation of the cost function can also be obtained using a Least-Squares (LS) fitting approach, instead of using TS from the nominal operating conditions. In that case, no derivatives are required, but several CFD analyses must be performed. Moreover, the cost function value at the nominal operating conditions obtained by CFD is usually different from the one predicted by LS fitting.

The FOSM method was applied to uncertainty propagation in aerodynamics in [13, 37, 43]. Comparisons between FOSM and SOSM methods are provided in [46]. Some robust optimization problems in aerodynamics have been addressed using the FOSM or SOSM methods to solve the problem (11) (MEV criterion) [23] or the two-objective problem (12) [37].

2.2.2 Radial Basis Functions

Radial Basis Functions (RBFs) are non-polynomial interpolation methods for scattered data [36]. They have been found to be very accurate for highly non-linear data in high dimension [6]. RBFs seek an approximation of the cost function of the form:

$$\tilde{\mathcal{J}}_{RBF}(\mathbf{x},\mathbf{a}) = \sum_{j=1}^{N_c} \omega_j(\mathbf{x})\ \phi(\|\mathbf{a}-\mathbf{a}_j\|), \tag{28}$$

where $(\mathbf{a}_j)_{j=1,\dots,N_c}$ are called RBFs centers. Several radial functions ϕ can be considered. For the present study a Gaussian function is employed:

$$\phi(r) = e^{-\frac{r^2}{s^2}}, \tag{29}$$

where s is a parameter called attenuation factor. Suppose that the cost function value is known for a set of N_c operating conditions that correspond to the RBF centers $(\mathbf{a}_i)_{i=1,\dots,N_c}$. Then, the weights $(\omega_j(x))_{j=1,\dots,N_c}$ are determined from the interpolation conditions:

$$\mathcal{J}(\mathbf{x},W(\mathbf{x},\mathbf{a}_i)) = \sum_{j=1}^{N_c} \omega_j(\mathbf{x})\ \phi(\|\mathbf{a}_i-\mathbf{a}_j\|) \quad i=1,\dots,N_c. \tag{30}$$

Thus, $(\omega_j(\mathbf{x}))_{j=1,\dots,N_c}$ is the solution of the following linear system:

$$\begin{pmatrix} \phi(0) & \phi(\|\mathbf{a}_1-\mathbf{a}_2\|) & \dots & \phi(\|\mathbf{a}_1-\mathbf{a}_{N_c}\|) \\ \phi(\|\mathbf{a}_2-\mathbf{a}_1\|) & \phi(0) & \dots & \phi(\|\mathbf{a}_2-\mathbf{a}_{N_c}\|) \\ \dots & \dots & \dots & \dots \\ \phi(\|\mathbf{a}_{N_c}-\mathbf{a}_1\|) & \phi(\|\mathbf{a}_{N_c}-\mathbf{a}_2\|) & \dots & \phi(0) \end{pmatrix} \begin{Bmatrix} \omega_1(x) \\ \omega_2(x) \\ \dots \\ \omega_{N_c}(x) \end{Bmatrix} = \begin{Bmatrix} \mathcal{J}(\mathbf{x},W(\mathbf{x},\mathbf{a}_1)) \\ \mathcal{J}(\mathbf{x},W(\mathbf{x},\mathbf{a}_2)) \\ \dots \\ \mathcal{J}(\mathbf{x},W(\mathbf{x},\mathbf{a}_{N_c})) \end{Bmatrix}. \tag{31}$$

The matrix of the system is obviously symmetric. It is also positive-definite if the RBFs centers $(\mathbf{a}_j)_{j=1,\dots,N_c}$ are distinct. One can notice that it is a full matrix. However, its dimension N_c is usually moderate in practice and its inversion is not time consuming. The attenuation factor s can be optimized or determined experimentally by the user. For the present study, the empirical formula is adopted [32]:

$$s = d_{max}(MN_c)^{-\frac{1}{M}}, \tag{32}$$

where M is the number of operating conditions under consideration $\mathbf{a} = (a^m)_{m=1,\dots,M}$ and d_{max} the maximum distance between RBFs centers.

To represent the cost function variability using this technique, some cost function evaluations are required, that correspond to the RBFs centers $(\mathbf{a}_j)_{j=1,\dots,N_c}$. These evaluations should be located in a region that depends on the PDF $\rho_{\mathbf{A}}$. This point will be discussed later for a practical application. Then, the approximation of the cost function is built by solving the system (31).

Once the approximation is computed, the cost function statistics can be estimated, either using numerical integration of integrals (15) and (16) or using Monte-Carlo estimates (19) and (20). The computational cost related to these estimations, which require only RBFs evaluations, is negligible.

2.3 Robust optimization problem

Since the computation of the cost function derivatives is a difficult task, if possible, the stochastic viewpoint is preferred in the present study. Then, for each design variable set, some cost function evaluations are performed to build a database, that is used to construct an approximation of the cost function as the operating conditions vary. Finally, a Monte-Carlo method is used to estimate the mean $\mathcal{M}_J$ and variance $\mathcal{S}_J^2$.

A two-objective optimization problem (12) should be solved to reduce the mean of the cost function as well as its variance. In the present study, this task is achieved by introducing a weighted sum of the two criteria as cost function:

$$\mathcal{J}_\lambda = \lambda \mathcal{M}_J + (1-\lambda)\mathcal{S}_J^2. \tag{33}$$

Using different weights allows to travel along the Pareto front. In the future, we plan to use evolutionary algorithms or game strategies dedicated to multi-objective problems.

3 Application to wing design with uncertain Mach number

3.1 Problem description

3.1.1 Testcase

The testcase considered here corresponds to the optimization of the wing shape of a business aircraft (courtesy of Piaggio Aero Ind.), for a transonic regime. The nominal operating conditions are defined by the free-stream Mach number $M_\infty = 0.83$ and the incidence $\alpha = 2°$. Initially, the wing section is supposed to correspond to the NACA 0012 airfoil. The initial wing shape is depicted in figure (2). The test-case is described in depth in [2].

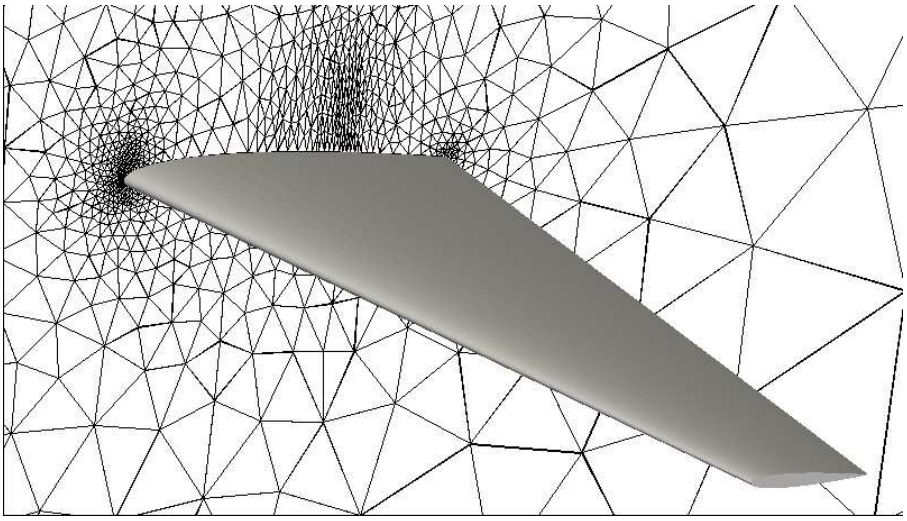

Figure 2: Initial wing shape and mesh in the symmetry plane.

We suppose that the free-stream Mach number is subject to random fluctuations. For simplicity, we assume that its PDF is Gaussian with a given mean μ_M and variance σ_M^2. The mean Mach number corresponds to the nominal Mach number $\mu_M = 0.83$ and its standard deviation is $\sigma_M = 0.0166$. Figure 3 depicts the Mach number distribution.

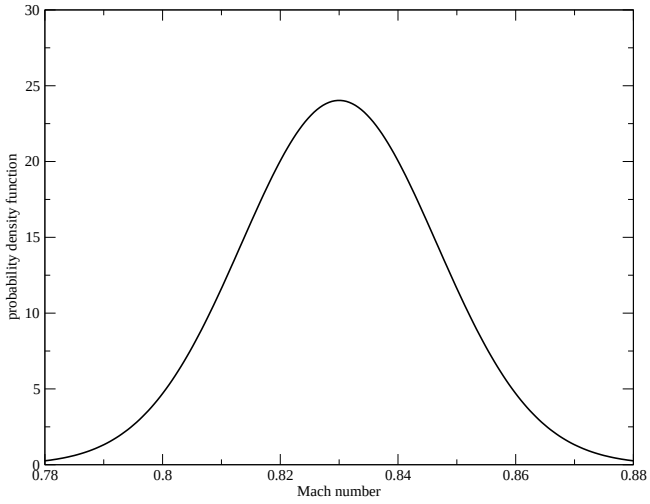

Figure 3: Probability density function of the free-stream Mach number.

The goal of the optimization is to reduce the drag coefficient C_D subject to the constraint that the lift coefficient C_L should not be lower than a prescribed value, that corresponds to $99,9\%$ of the lift for the initial shape at nominal operating conditions. The constraint is taken into account using a penalization approach. The aerodynamic coefficients are computed using an inviscid flow solver. The mesh employed counts 31124 nodes

and includes a refined area to accurately capture the shock wave (see figure 2). The next sections describe the shape parameterization, the flow solver and the optimization algorithm considered for this study.

3.1.2 Parameterization

The shape deformation is parameterized using the Free-Form Deformation (FFD) approach. The FFD technique originates from the Computer Graphics field [39]. It allows the deformation of an object in a 2D or 3D space, regardless of the representation of this object. Instead of manipulating the surface of the object directly, by using classical B-Splines or Bézier parameterization of the surface, the FFD techniques defines a deformation field over the space embedded in a lattice which is built around the object. By transforming the space coordinates inside the lattice, the FFD technique deforms the object, regardless of its geometrical description.

More precisely, consider a three-dimensional hexahedral lattice embedding the object to be deformed. Figure (4) shows an example of such a lattice built around a realistic wing. A local coordinate system (ξ, η, ζ) is defined in the lattice, with $(\xi, \eta, \zeta) \in [0,1] \times [0,1] \times [0,1]$. During the deformation, the displacement Δq of each point q inside the lattice is here defined by a third-order Bézier tensor product:

$$\Delta q = \sum_{i=0}^{n_i} \sum_{j=0}^{n_j} \sum_{k=0}^{n_k} B_i^{n_i}(\xi_q) B_j^{n_j}(\eta_q) B_k^{n_k}(\zeta_q) \Delta P_{ijk}. \tag{34}$$

$B_i^{n_i}$, $B_j^{n_j}$ and $B_k^{n_k}$ are the Bernstein polynomials of order n_i, n_j and n_k (see for instance [18]):

$$B_p^n(t) = C_n^p \, t^p \, (1-t)^{n-p}. \tag{35}$$

$(\Delta P_{ijk})_{0 \le i \le n_i, 0 \le j \le n_j, 0 \le k \le n_k}$ are weighting coefficients, or control points displacements, which are used to monitor the deformation and are considered as design variables during the shape optimization procedure.

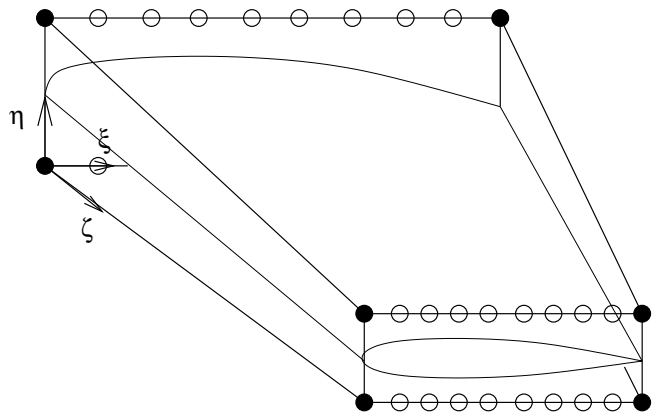

Figure 4: Example of FFD lattice around a wing.

The FFD technique described above is well suited to complex shape optimization, thanks to the following properties:

- the initial shape can be exactly represented (no deformation occurs when all weighting coefficients are zero) ;
- the deformation is performed whatever the complexity of the shape (this is a free-form technique) ;
- geometric singularities can be taken into account (the initial shape including its singularities is deformed) ;
- the smoothness of the deformation is controlled (the deformation is ruled by Bernstein polynomials) ;
- the number of design variables depends on the user's choice (the deformation is independent of the shape itself) ;
- it nicely deals with multi-level representation (thanks to the Bézier degree elevation property).

The FFD technique is implemented in the shape optimization procedure and is used to control the shape deformation for complex applications in aerodynamics (see [11] for details).

The FFD lattice is built around the wing with ξ, η and ζ in the chordwise, spanwise and thickness directions respectively. The lattice is chosen in order to fit the planform of the wing (see figure 4). Then, the leading and trailing edges are kept fixed during the optimization by freezing the control points that correspond to $i = 0$ and $i = n_i$. On figure 4, filled markers correspond to frozen control points, whereas empty markers correspond to moving control points. Moreover, control points are only moved vertically. The parameterization used in the present study corresponds to $n_i = 9$, $n_j = 1$ and $n_k = 1$ and counts $(10 - 2) \times 2 \times 2 = 32$ degrees of freedom. The FFD method is also used to deform the mesh in accordance with the boundary displacement.

3.1.3 Aerodynamic analysis

Modeling This study is restricted to three-dimensional inviscid compressible flows governed by the Euler equations. Then, the state equations can be written in the conservative form :

$$\frac{\partial W}{\partial t} + \frac{\partial F_1(W)}{\partial x} + \frac{\partial F_2(W)}{\partial y} + \frac{\partial F_3(W)}{\partial z} = 0, \tag{36}$$

where W are the conservative flow variables $(\rho, \rho u, \rho v, \rho w, E)$, with ρ the density, $\overrightarrow{U} = (u, v, w)$ the velocity vector and E the total energy per unit of volume. $\overrightarrow{F} = (F_1(W), F_2(W), F_3(W))$ is the vector of the convective fluxes, whose components are given by :

$$F_1(W) = \begin{pmatrix} \rho u \\ \rho u^2 + p \\ \rho uv \\ \rho uw \\ u(E+p) \end{pmatrix} \quad F_2(W) = \begin{pmatrix} \rho v \\ \rho uv \\ \rho v^2 + p \\ \rho vw \\ v(E+p) \end{pmatrix} \quad F_3(W) = \begin{pmatrix} \rho w \\ \rho uw \\ \rho vw \\ \rho w^2 + p \\ w(E+p) \end{pmatrix}. \tag{37}$$

The pressure p is obtained from the perfect gas state equation :

$$p = (\gamma - 1)(E - \frac{1}{2}\rho \| \overrightarrow{U} \|^2), \tag{38}$$

where $\gamma = 1.4$ is the ratio of the specific heat coefficients.

Spatial discretization An unstructured mesh, composed of 31124 nodes and 173 445 tetrahedral elements, is generated around the wing, including a refined area in the vicinity of the shock (see figure (2)). Provided that the flow domain Ω is discretized by a tetrahedrization $\mathcal{T}_h$, a discretization of equation (36) at the mesh node s_i is obtained by integrating (36) over the volume C_i, that is built around the node s_i by joining barycenters of the tetrahedra and triangles containing s_i and midpoints of the edges adjacent to s_i :

$$Vol_i \frac{\partial W_i}{\partial t} + \sum_{j \in N(i)} \Phi(W_i, W_j, \overrightarrow{\sigma}_{ij}) = 0, \tag{39}$$

where W_i represents the cell averaged state and Vol_i the volume of the cell C_i. $N(i)$ is the set of the neighboring nodes. $\Phi(W_i, W_j, \overrightarrow{\sigma}_{ij})$ is an approximation of the integral of the fluxes (37) over the boundary ∂C_{ij} between C_i and C_j, which depends on W_i, W_j and $\overrightarrow{\sigma}_{ij}$ the integral of a unit normal vector over ∂C_{ij}. These numerical fluxes are evaluated using upwinding, according to the approximate Riemann solver of Roe :

$$\Phi(W_i, W_j, \overrightarrow{\sigma}_{ij}) = \frac{\overrightarrow{F}(W_i) + \overrightarrow{F}(W_j)}{2} \cdot \overrightarrow{\sigma}_{ij} - |A_R(W_i, W_j, \overrightarrow{\sigma}_{ij})| \frac{W_j - W_i}{2}. \tag{40}$$

A_R is the jacobian matrix of the fluxes for the Roe average state and verifies:

$$A_R(W_i, W_j, \overrightarrow{\sigma}_{ij})(W_j - W_i) = (\overrightarrow{F}(W_j) - \overrightarrow{F}(W_i)) \cdot \overrightarrow{\sigma}_{ij}. \tag{41}$$

A high order scheme is obtained by interpolating linearly the physical variables from s_i to the midpoint of $[s_i s_j]$, before equation (40) is employed to evaluate the fluxes. Nodal gradients are obtained from a weighting average of the P1 Galerkin gradients computed on each tetrahedron containing s_i. In order to avoid spurious oscillations of the solution in the vicinity of the shock, a slope limitation procedure using the Van-Albada limiter is introduced. The resulting discretization scheme exhibits a third order accuracy in the regions where the solution is regular.

Time integration A first order implicit backward scheme is employed for the time integration of (39), which yields :

$$\frac{Vol_i}{\Delta t}\delta W_i + \sum_{j\in N(i)} \Phi(W_i^{n+1}, W_j^{n+1}, \overrightarrow{\sigma}_{ij}) = 0, \tag{42}$$

with $\delta W_i = W_i^{n+1} - W_i^n$. Then, the linearization of the numerical fluxes provides the following integration scheme :

$$\left(\frac{Vol_i}{\Delta t} + J_i^n\right)\delta W_i = -\sum_{j\in N(i)} \Phi(W_i^n, W_j^n, \overrightarrow{\sigma}_{ij}). \tag{43}$$

Here, J_i^n is the Jacobian matrix of the first order numerical fluxes, whereas the right hand side of (43) is evaluated using high order approximations. The resulting integration scheme provides a high order solution of the steady problem.

3.1.4 Optimization algorithm

The optimization algorithm used in the present study is a Particle Swarm Optimization (PSO) approach, that is employed in conjunction with a multi-level parameterization strategy. The method is described in depth in [12].

PSO algorithm was first introduced by Kennedy and Eberhart [28], as a simplified social model. It mimics the behavior of birds flocking and is based on underlying rules that enable sudden direction changes, scattering, regrouping, etc. These moves are motivated in nature by food seeking or predators avoiding and can be implemented in a simple algorithm for global optimization purpose [19, 40, 45].

The algorithm consists in building the trajectories of the particles of a swarm in the search space of dimension n. These trajectories are adjusted dynamically to take into account the information collected about the cost function value. Consider a set of p particles that constitutes the swarm. The location of each particle i at the time step (k) is determined by its coordinates $(\mathbf{x}_i^{(k)})_{1\leq i\leq p} \in \Re^n$. The behavior of each particle is then characterized by its velocity $(\mathbf{v}_i^{(k)})_{1\leq i\leq p} \in \Re^n$. Initially, particule locations are randomly chosen in a given interval $[\mathbf{x}^{MIN}, \mathbf{x}^{MAX}]$. Velocities are initialized randomly with a maximum modulus $(\mathbf{x}^{MAX} - \mathbf{x}^{MIN})/2$ Hence, particles can cover half of the initialization interval during the first time step. At each time step, the velocity of each particle is then updated according to some criteria:

- the particle inertia : parameter ω ;
- the best location ever found by the particle i : $(\mathbf{x}_i^\star)_{1\leq i\leq p}$ (individual memory) ;
- the best location ever found by the swarm : $\mathbf{x}^\star$ (collective memory).

Hence, the velocity of the particle i is defined in practice by:

$$\mathbf{v}_i^{(k)} = \underbrace{\omega \mathbf{v}_i^{(k-1)}}_{\text{term } ①} + \underbrace{c_1 r_1 (\mathbf{x}_i^\star - \mathbf{x}_i^{(k)})}_{\text{term } ②} + \underbrace{c_2 r_2 (\mathbf{x}^\star - \mathbf{x}_i^{(k)})}_{\text{term } ③} \quad 1 \leq i \leq p, \tag{44}$$

where r_1 and r_2 are uniformly distributed random numbers $\in [0, 1]$. The term ① corresponds to the inertia, whereas the terms ② and ③ correspond to attractions towards the individual and collective memories. The particle location is then updated by time integration during a time step of length unity:

$$\mathbf{x}_i^{(k+1)} = \mathbf{x}_i^{(k)} + \mathbf{v}_i^{(k)} \quad 1 \leq i \leq p. \tag{45}$$

c_1 and c_2 in (44) are called trust coefficients and are set to the value two [28]. Then, the two related attraction terms in (44) yield the particle to overfly the locations corresponding to the individual and collective memories with a probability one half every time step. This algorithm does not exactly correspond to the original one proposed by Kennedy and Eberhart [28], which did not use inertia. Moreover, velocity were updated by taking into account the best location found by the swarm at each time. The use of the inertia term was proposed by Shi and Eberhart [40], whereas the use of the best location ever found by the swarm to update the velocity was introduced by Fourie and Groenwold [19]. These works reported some improvements related to these modifications.

Moreover, these works reported the critical influence of the inertia parameter ω on the results. Indeed, for large ω values the exploration in the search space is promoted, whereas a small ω value favors a straight

convergence towards the best locations ever found. A mathematical analysis of the dynamical system, including stability conditions, can be found in the work of Clerc and Kennedy [8]. Shi and Eberhart [40] proposed practically that ω value be selected such that $\omega \in [0.8, 1.4]$. They also reported improved convergence rates when ω is decreased linearly during the optimization. The present implementation is based on a dynamic update of ω proposed by Fourie and Groenwold [19]. A starting ω^0 is chosen with a quite large value in order to promote an exploratory search. Then, its value is decreased by a factor α if no improved solution is found within h consecutive time steps: Therefore, if the exploratory search fails, the convergence towards the best locations ever found is promoted.

Some authors include in the basic algorithm a craziness operator whose role is to add random perturbations. This operator is inspired from the mutation operator in GAs. First, Kennedy and Eberhart [28] proposed to randomly perturbate the velocity of some particles, but they concluded that this operator was not mandatory. Fourie and Groenwold [19] reintroduced a craziness operator that randomly modifies the velocities with a predetermined probability and with a decreasing amplitude of perturbation. Venter and Sobieski [45] also used such an operator, but they decided to perturbate both particles location and velocity. In the current work, a craziness operator is implemented in the spirit of Fourie and Groenwold operator. Especially, a probability of craziness $p_c \in [0, 1]$ is predetermined. Then, at each time step and for each particle, the velocity direction is randomly modified with the probability p_c, but the velocity modulus is kept constant. Therefore, large random perturbations occur at the beginning of the optimization procedure, which promote random global search, whereas small random perturbations are performed when the swarm is close to the solution, which promote random local search. This approach is inspired from the so-called non-uniform mutation operator in GAs [30].

Finally, Shi and Eberhart [40] proposed to introduce a maximum velocity value v^{MAX} for stability purpose and observed an improvement of the convergence rate. This strategy is also used in the present study.

Finally, the algorithm implemented in the current study can be described as follows:

1. initialize randomly the locations $(\mathbf{x}_i^{(0)})_{1 \leq i \leq p}$ in the interval $[\mathbf{x}^{MIN}, \mathbf{x}^{MAX}]$;
   initialize the inertia $\omega^{(0)}$;
   $k \leftarrow 0$;
2. begin time step k ;
3. estimate the fitness of all particles $1 \leq i \leq p$;
4. update the individual memory $(\mathbf{x}_i^\star)_{1 \leq i \leq p}$ and the collective memory $\mathbf{x}^\star$;
5. Check if the inertia should be updated
   $$\text{If } \mathcal{J}(\mathbf{x}^\star)|_k = \mathcal{J}(\mathbf{x}^\star)|_{k-h} \text{ then } \omega^{(k)} = \alpha\, \omega^{(k-1)};$$
6. compute the velocity of the particles
   $$\mathbf{v}_i^{(k)} = \omega^{(k)} \mathbf{v}_i^{(k-1)} + c_1 r_1 (\mathbf{x}_i^\star - \mathbf{x}_i^{(k)}) + c_2 r_2 (\mathbf{x}^\star - \mathbf{x}_i^{(k)}) \quad 1 \leq i \leq p;$$
7. check if the velocities are not above $\mathbf{v}^{MAX}$;
8. apply craziness with a probability p_c : random perturbation of the velocity with a constant velocity modulus
9. update the location of the particles
   $$\mathbf{x}_i^{(k+1)} = \mathbf{x}_i^{(k)} + \mathbf{v}_i^{(k)};$$
10. if termination condition reached then stop ;
    else $k \leftarrow k + 1$ and goto (2);

The main weakness of such semi-stochastic optimizers is that the number of cost function evaluations increase dramatically with the dimension of the problem. This observation has motivated the development of an algorithm that relies on a multi-level parameterization [12]. It consists in using a parameterization of the shapes that uses a progressively increasing number of design variables.

Numerical parameters for the PSO algorithm are set using results from the literature and prior tests:

$T^{MAX} = 200$	max number of time steps
$\omega^0 = 1.2$	initial inertia
$h = 3$	inertia reduction criterion
$\alpha = 0.98$	inertia reduction rate
$c_1 = c_2 = 2$	trust coefficients
$p_c = 0.05$	craziness probability
$\mathbf{v}^{MAX} = 0.25\ (\mathbf{x}^{MAX} - \mathbf{x}^{MIN})$	maximum velocity

For all the computations, the number of particles is $p = 30$.

3.2 Single-point optimization

We first solve a deterministic optimization problem, with fixed operating conditions. Hence, the Mach number is supposed to have its nominal value $M_\infty = 0.83$. An optimal shape is obtained by minimizing the drag coefficient constrained by a minimum lift coefficient.

We now analyze the variation of the aerodynamic coefficients for the optimal design found, as the Mach number varies around its nominal value. The next table compares the aerodynamic coefficients for Mach numbers equal to 0.81, 0.83 and 0.85:

Mach number	Drag coef.	Lift coef.
0.81	0.01029	0.2929
0.83 (nominal)	0.01139	0.3188
0.85	0.01811	0.3512

As can be seen in the above table, the drag coefficient abruptly increases as the Mach number goes beyond its nominal value. One can also notice that the lift coefficient decreases significantly if the Mach number is below its nominal value. Figure 5 shows a comparison of the Mach number fields at the wing surface for the three Mach numbers under consideration. The optimization procedure yields a wing shape that minimizes the shock wave at nominal Mach number. Then, the intensity of the shock does not change significantly as the Mach number varies from 0.81 to 0.83. However, at Mach number 0.85, the shock wave strongly reinforces. It results an increase of the drag coefficient.

The behavior of the initial wing (NACA 0012 section) and the optimal wing shape at nominal Mach number is systematically analyzed for a Mach number that varies in the interval $[\mu_M - 3\sigma_M, \mu_M + 3\sigma_M]$. Twenty-one flow analyses are performed. Results are depicted in figure 6. As expected, the optimum design is fully adapted to the nominal Mach number: the drag coefficient is maintained at a low value until the nominal Mach number and then increases abruptly. Figure 7 depicts the relative drag reduction with respect to the Mach number:

$$r = \frac{C_D^\star - C_D^{(0)}}{C_D^{(0)}}, \tag{46}$$

where $C_D^\star$ is the drag coefficient for the optimal wing shape and $C_D^{(0)}$ for the initial wing shape. As expected, the drag reduction is maximum at the nominal Mach number.

The optimization of the wing shape at various Mach numbers yields a set of shapes, that are all adapted to a precise Mach number. Figure 8 shows the drag variation for shapes optimized at $M_\infty = 0.82$, $M_\infty = 0.84$, $M_\infty = 0.86$ and $M_\infty = 0.88$. Each of these shapes is optimum for a precise Mach number but has not a satisfactory behavior as the Mach number varies in the whole interval $[\mu_M - 3\sigma_M, \mu_M + 3\sigma_M]$. The relative drag reduction depicted in figure 9 shows that each optimization exercise adapts the wing shape to the particular operating conditions used during the optimization. One can observe that the wing shapes obtained have different characteristics (figure 10).

These observations motivate the robust design of the wing subject to uncertain Mach number. Then, the classical problem (1) is replaced by the robust formulation (12). Our purpose is now to reduce the mean drag as well as its variance. The lift constraint is now: the probability for the lift to be higher than the prescribed value should be higher than $p = 0.95$.

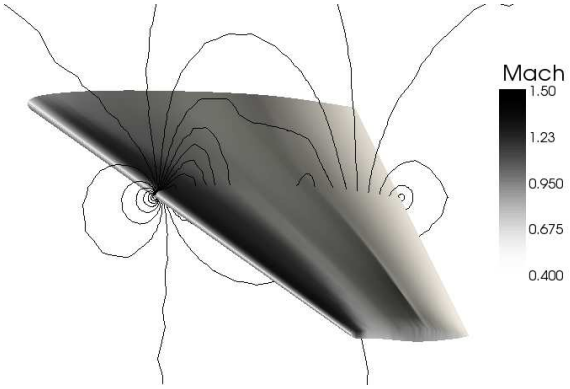

(a) $M_\infty = 0.81$

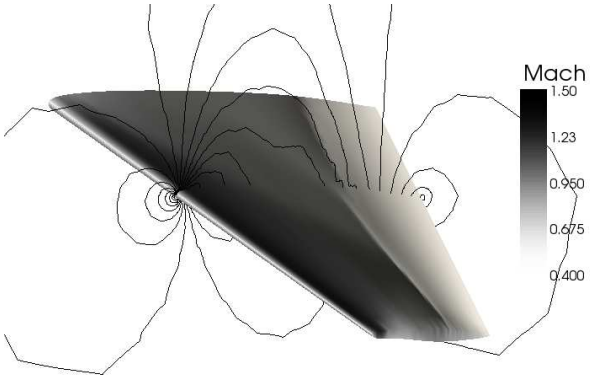

(b) $M_\infty = 0.83$

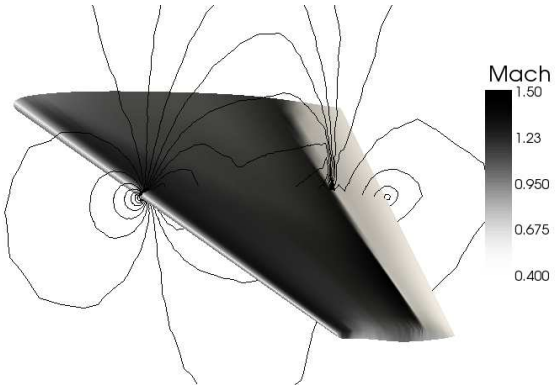

(c) $M_\infty = 0.85$

Figure 5: Mach number field at the wing surface and iso-Mach contours for a shape optimized at nominal Mach number; top: Mach number 0.81; middle: Mach number 0.83 (nominal); bottom: Mach number 0.85.

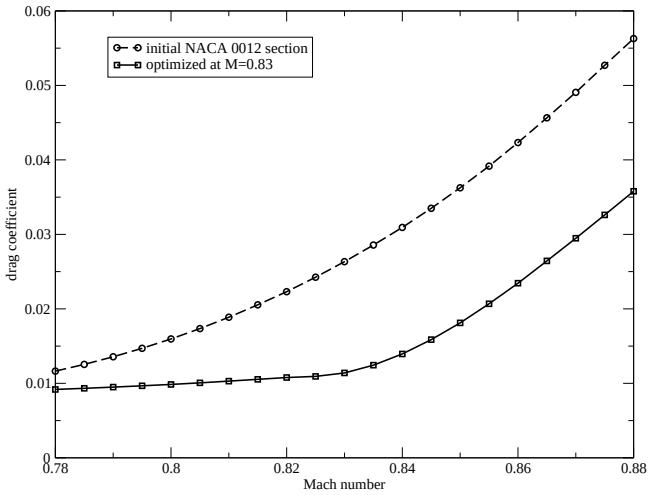

Figure 6: Drag variation for fluctuating Mach number: initial design and optimum design at nominal Mach number (0.83).

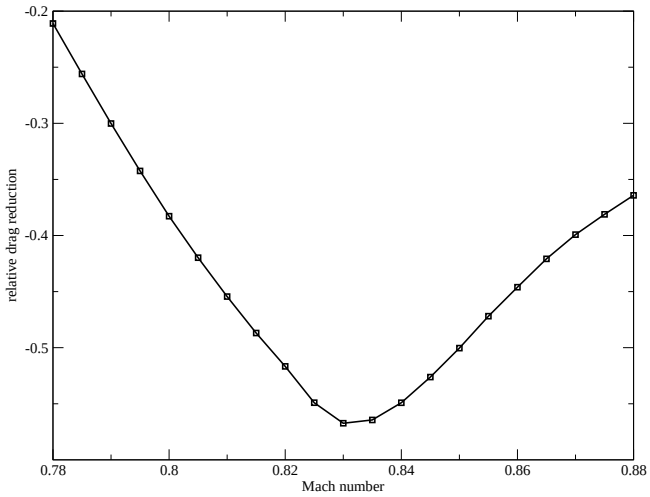

Figure 7: Relative drag reduction for a wing shape optimized at nominal Mach number.

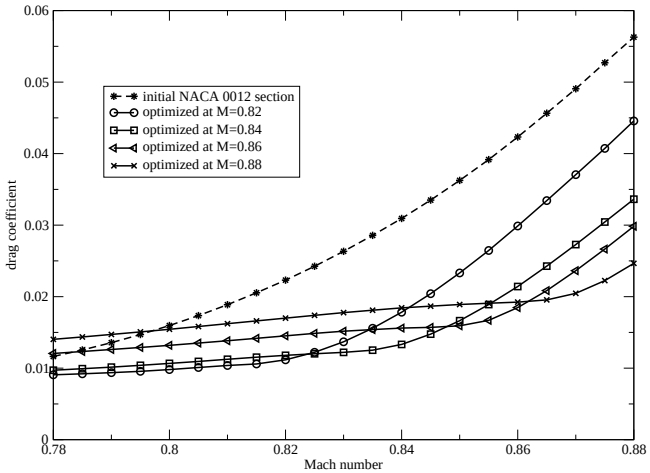

Figure 8: Drag variation for fluctuating Mach number: initial design and optimum designs at different Mach number values.

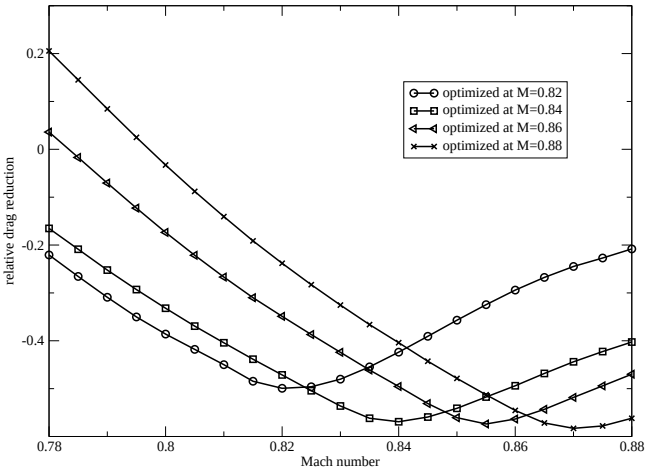

Figure 9: Relative drag reduction for a wing shape optimized at different Mach number values.

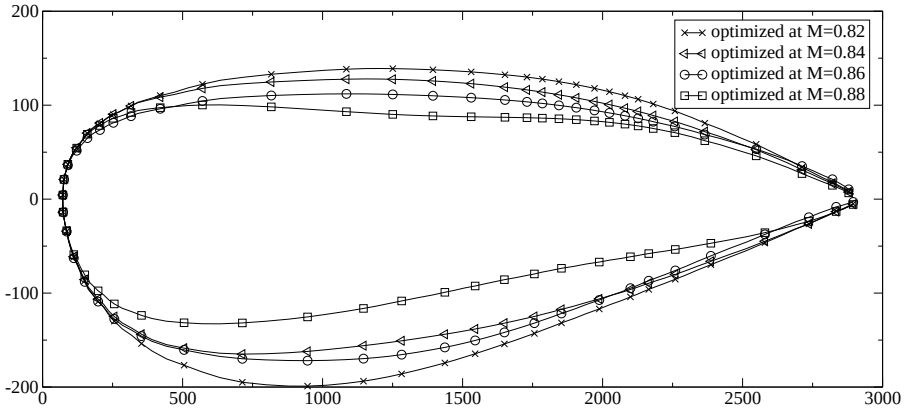

Figure 10: Comparison of the wing shape at the root section: optimum designs at different Mach number values.

3.3 Study of uncertainty propagation

We study in this section the uncertainty propagation. We try to determine the PDF of the drag coefficient for the optimum design found previously, yielding its mean and its variance. We adopt the stochastic viewpoint described previously. Then, models of the aerodynamic coefficients are constructed and used to estimate the statistics in a Monte-Carlo approach. We consider linear and quadratic approximations of the aerodynamic coefficients, as well as RBFs. Polynomial approximations are not constructed using Taylor series and sensitivity analysis, but using a least-squares fitting method.

First, a reference result is obtained by using the previous twenty-one analyses to construct a very fine model (RBFs) and propagate the uncertainty by the Monte-Carlo approach. This reference result is then compared to the use of three possible models that rely on $N_c = 5$ points in the database: linear fitting, quadratic fitting and RBFs. The five points are uniformly distributed in the interval $[\mu_M - 3\sigma_M, \mu_M + 3\sigma_M]$. Figure 11 shows the data fitting for the linear and quadratic least-squares approximations. The resulting PDFs are compared to the reference result in figures 12 and 13.

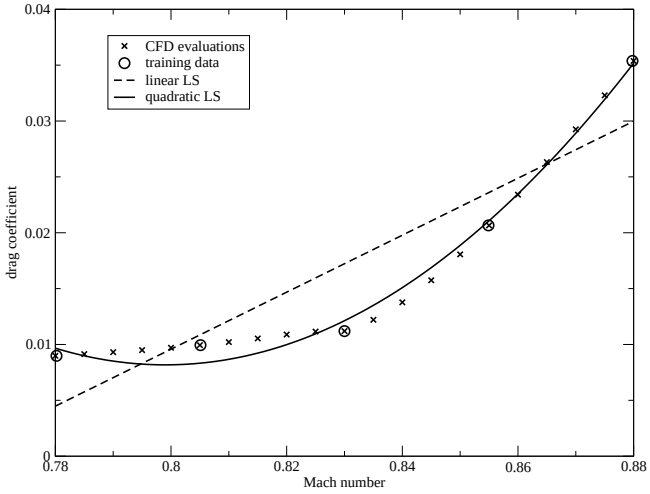

Figure 11: Five-point fitting using linear and quadratic least-squares approximation.

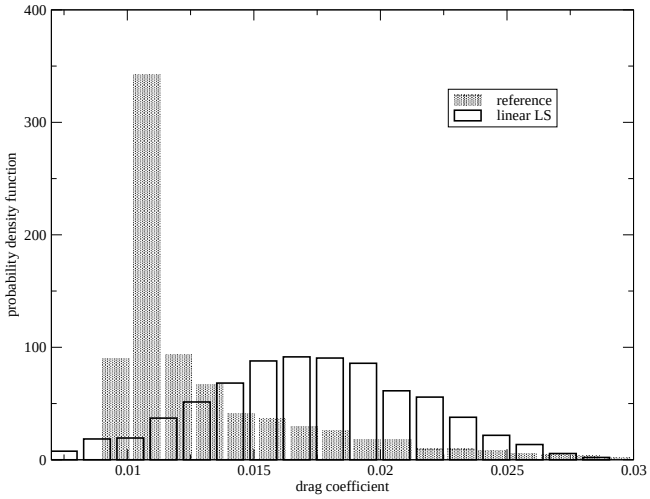

Figure 12: Probability density function of the drag coefficient: reference result compared to linear fitting.

The linear fitting has obviously a poor accuracy and the resulting PDF is Gaussian. This is far from the reference result, for which the PDF has a more complex shape and is characterized by a peak at low drag values. The quadratic fitting is closer to the CFD calculations for high Mach numbers. Then, the tail of the PDF is quite well reproduced. However, the peak description is not satisfactory.

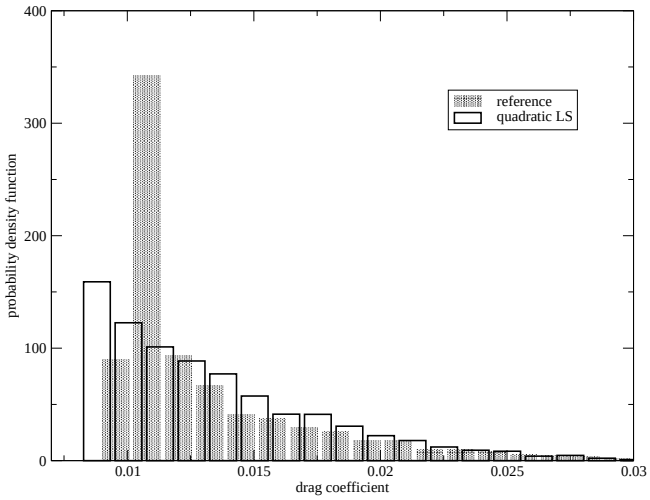

Figure 13: Probability density function of the drag coefficient: reference result compared to quadratic fitting.

Figures 14 and 15 depict the results obtained with RBFs. Obviously, the capability of RBFs to fit the data is better than that of linear or quadratic functions. The resulting PDF is similar to the reference PDF, except for the peak intensity. This is due to the discrepancy that can be observed between the RBFs fitting and the CFD results at Mach number 0.82. To accurately represent the curvature in this region, the database must be enlarged. Using $N_c = 7$ points in the database provides satisfactory results (figures 16 and 17). This choice is adopted for the next computations. Table 1 compiles the statistics obtained for the different cases.

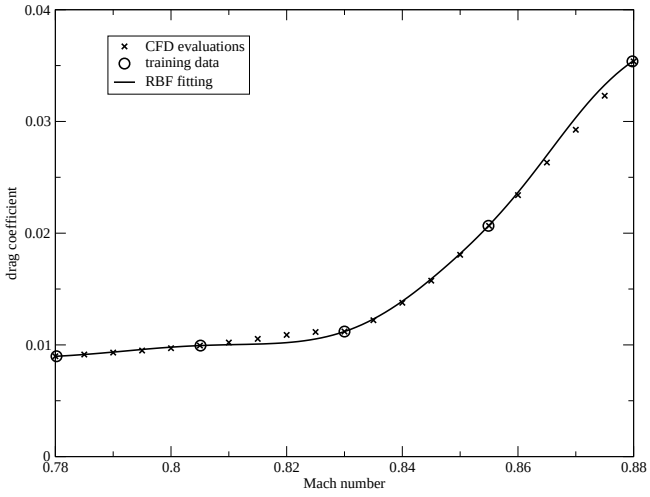

Figure 14: Five-point fitting using RBFs.

Case	Mean	Variance
Reference	0.013154	1.5658E-05
Linear fit (5 pts)	0.017229	1.7953E-05
Quadratic fit (5 pts)	0.013262	1.9482E-05
RBFs (5 pts)	0.013029	1.7229E-05
RBFs (7 pts)	0.013068	1.5899E-05

Table 1: Statistics for the drag obtained with the different methods.

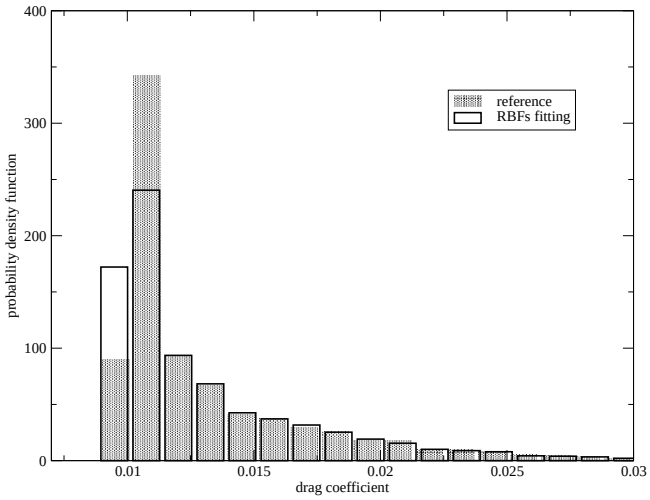

Figure 15: Probability density function of the drag coefficient: reference result compared to RBFs (5 points).

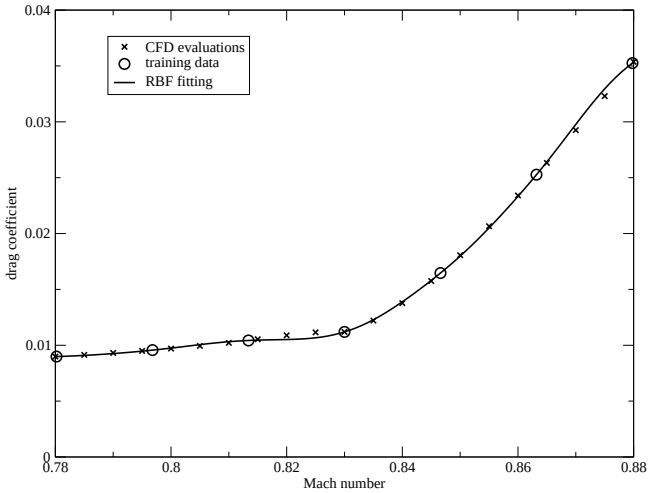

Figure 16: Seven-point fitting using RBFs.

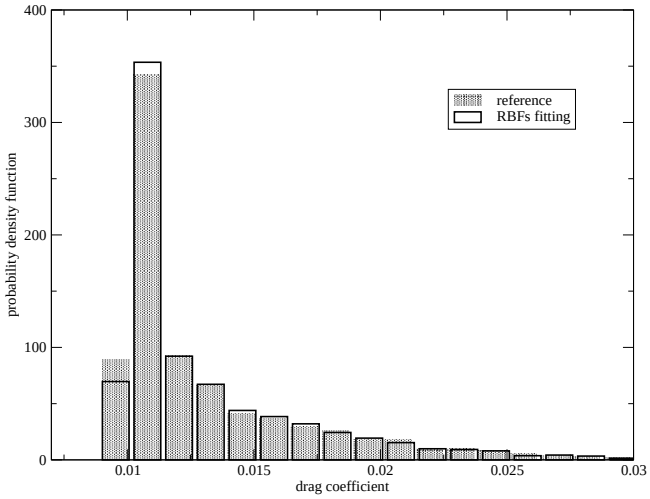

Figure 17: Probability density function of the drag coefficient: reference result compared to RBFs (7 points).

3.4 Results for robust design

Once uncertainty propagation relies on a safe basis, the robust optimization problem (12) can be addressed. In the present study, the two-objective problem is solved using a composite cost function, which is the weighted sum of the mean and variance.

3.4.1 Pareto front

Five optimization exercises are solved using different weights to draw the Pareto front (see figure 18). The results corresponding to these five optimization exercises are summarized in table 2.

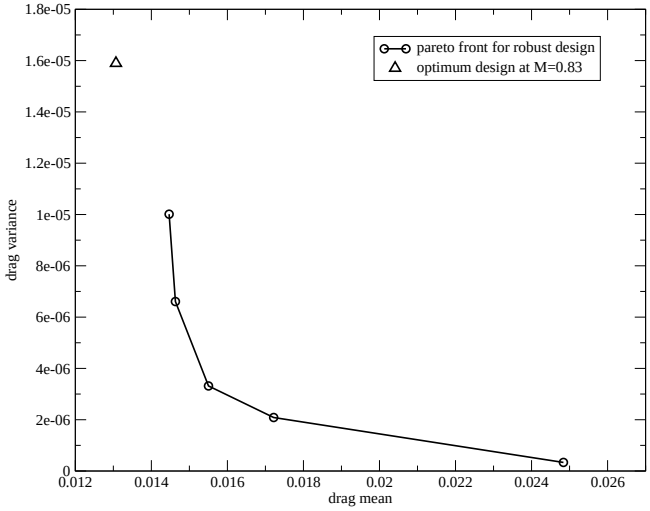

Figure 18: Pareto front for the two-objective robust design problem.

Weight for the mean	Weight for the variance	Mean	Variance	Constraint probability
1.0	0.0	0.0144	1.001E-05	0.9504
0.75	0.25	0.0146	6.607E-06	0.9501
0.5	0.5	0.0155	3.316E-06	0.9504
0.25	0.75	0.0172	2.085E-06	0.9512
0.0	1.0	0.0248	3.355E-07	0.9576

Table 2: Statistics for the different robust optimization exercises.

One can notice that the design optimized at nominal Mach number has a lower mean drag than the design found by minimizing the mean drag. It is due to the fact that the optimum design at nominal Mach number does not respect the lift constraint in the probabilistic sense. For this design, the probability to reach the prescribed lift value is only 0.5057.

3.4.2 Drag coefficient variations

The evolution of the drag coefficient as the Mach number varies can be seen in figure 19 for three points on the Pareto front. These results are obtained by performing *a posteriori* twenty-one CFD analyses in the interval $[\mu_M - 3\sigma_M, \mu_M + 3\sigma_M]$ for the three designs under consideration. The corresponding PDFs are depicted on figure 20. As can be seen, a design is found, for which the drag is almost constant over the interval $[\mu_M - 3\sigma_M, \mu_M + 3\sigma_M]$. However, its mean drag is poor, since it is not taken into account during the optimization. On the contrary, a second design optimizes the mean drag, but exhibits a significant drag increase for high Mach numbers. Finaly, a trade-off design is shown, for which the mean is slightly degraded but the drag fluctuations are moderate. The comparison of the PDFs clearly shows the characteristics of these different designs.

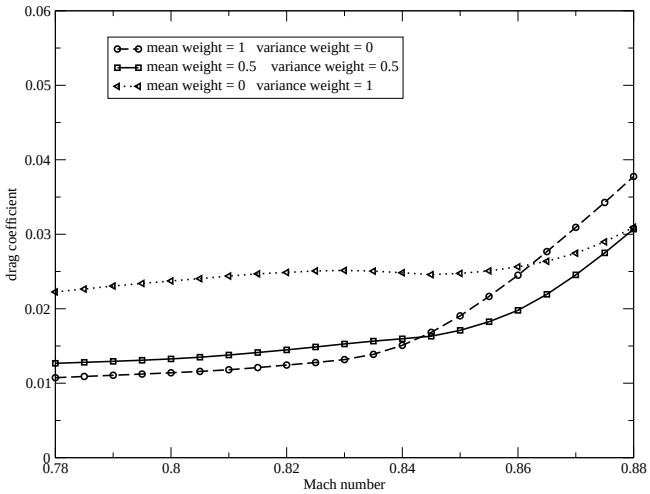

Figure 19: Drag variation for fluctuating Mach number: robust designs from the Pareto front.

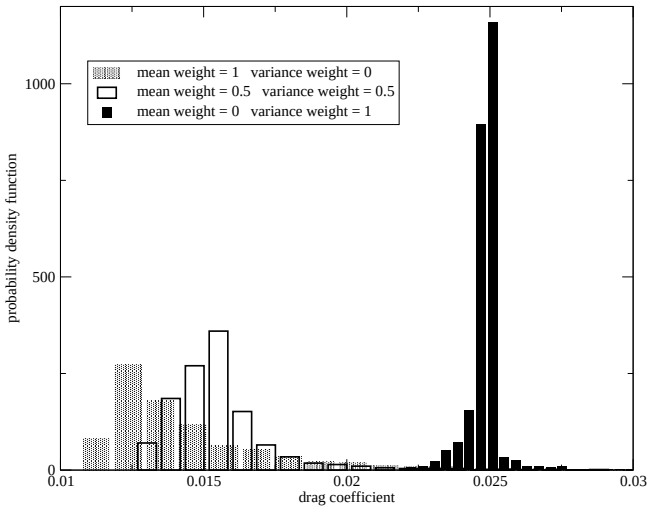

Figure 20: Probability density functions for the drag coefficient: robust designs from the Pareto front.

3.4.3 A posteriori validation

The twenty-one CFD analyses performed for the robust design found (weights of value 0.5) are used for an *a posteriori* validation of the uncertainty analysis. These CFD analyses provide a reference model for uncertainty propagation, that is compared to the seven- point RBFs fitting used during the optimization procedure. Figure 21 shows that the RBFs fitting using seven points is quite accurate. A comparison of the PDFs obtained is depicted in figure 22. As can be seen, a satisfactory agreement between the RBFs model and the reference model is obtained. The table 3 compares the corresponding mean and variance estimated. The accuracy of the statistics estimation for the robust design found is fine, which yields an *a posteriori* validation of the robust design optimization procedure.

Model	Mean	Variance
Reference	0.0155	3.3120E-06
RBFs	0.0155	3.3163E-06

Table 3: Statistics for the drag for the robust design obtained with the reference model and the seven-point RBFs fitting.

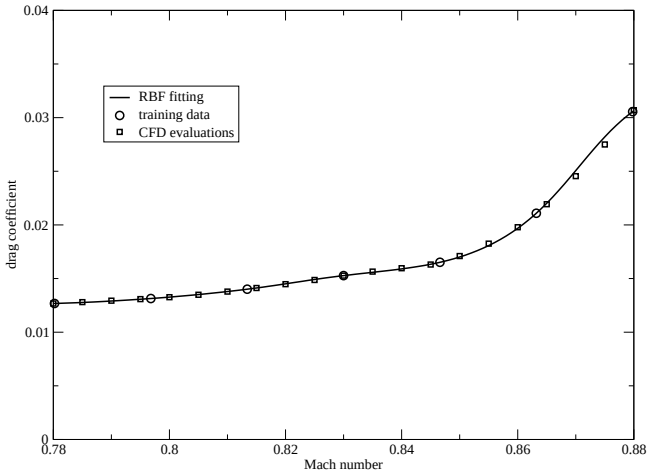

Figure 21: Seven-point fitting using RBFs for the robust design.

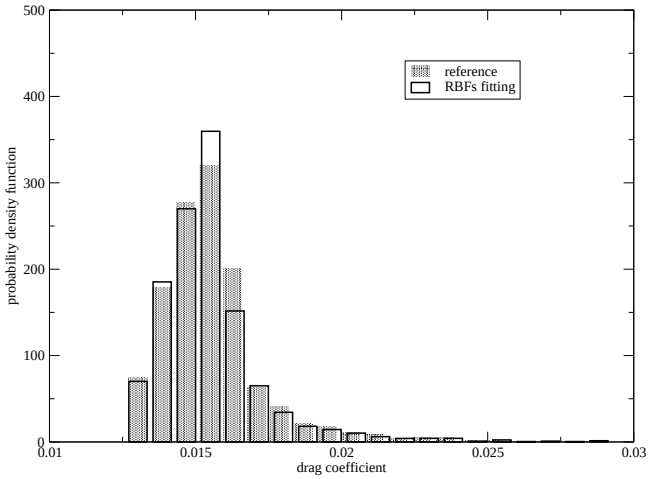

Figure 22: Probability density functions for the drag coefficient: reference result for the robust design compared to RBFs (7 points).

3.4.4 Shape comparison

A comparison of the wing shapes at the root section is depicted in figure 23, for the optimum design at nominal Mach number and three robust designs from the Pareto front. One can notice that the pressure side of the robust design is more and more flat as the weight for the variance increases.

3.4.5 Flow analysis

Figure 24 shows a comparison of the Mach number fields at the wing surface for the robust design found (weights of value 0.5) as the Mach number varies. This figure has to be compared to the figure 5 which depicts the same results for the wing shape optimized at nominal Mach number. One can notice that the flow field evolves progressively as the Mach number varies. Contrary to the latter case, the birth of a strong shock is not observed when the Mach number increases from 0.83 to 0.85. Thus, the wing shape is more "robust" with respect to Mach number variations.

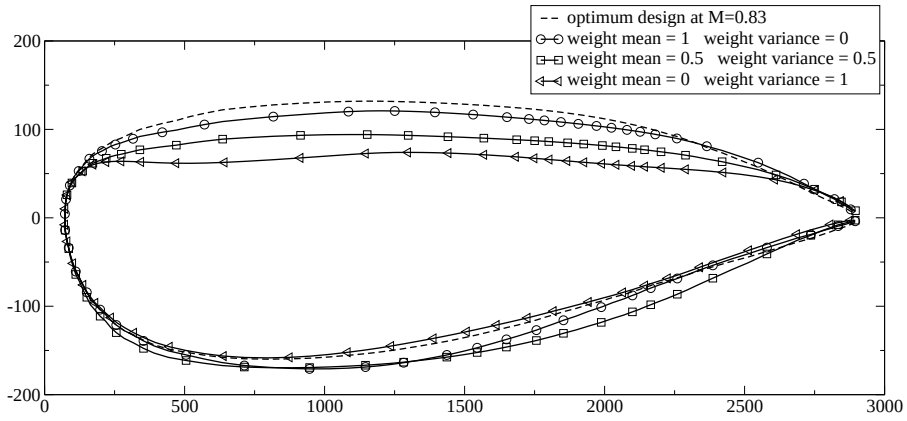

Figure 23: Comparison of the wing shape at the root section: optimum design at nominal Mach number and robust designs from the Pareto front.

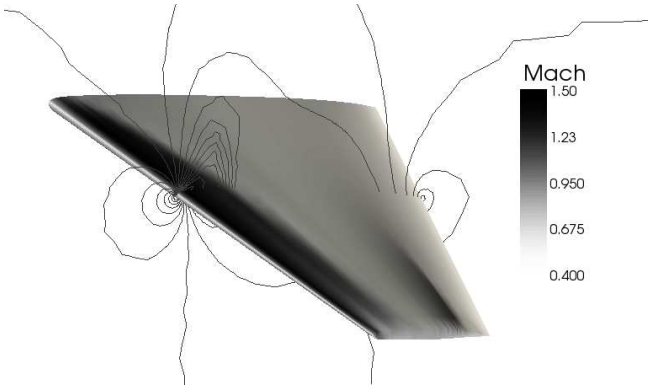

(a) $M_\infty = 0.81$

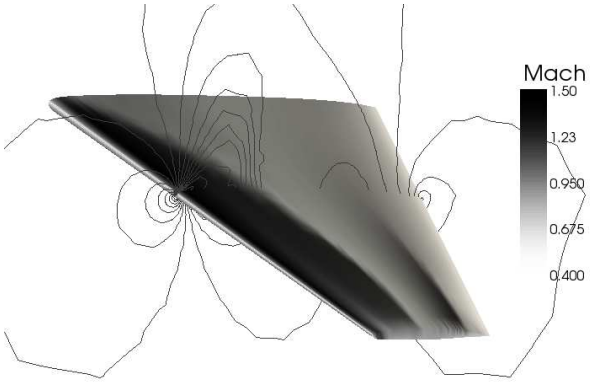

(b) $M_\infty = 0.83$

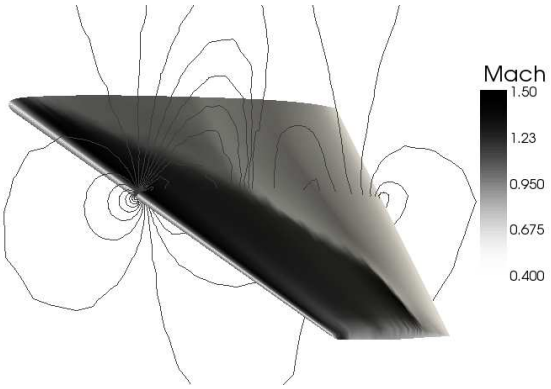

(c) $M_\infty = 0.85$

Figure 24: Mach number field at the wing surface and iso-Mach contours for the robust design; top: Mach number 0.81; middle: Mach number 0.83 (nominal); bottom: Mach number 0.85.

Conclusion

The problem of aerodynamic shape optimization with uncertain operating conditions is addressed in this paper. To overcome the difficulty related to the high computational cost required by robust design, a two-level modeling strategy is proposed, that relies on the use of meta-models, such as radial basis functions, to estimate statistics in a Monte-Carlo method. A robust optimization problem is then solved by minimizing the mean and the variance of the cost function.

This methodology is demonstrated for a realistic wing design in transonic regime. A robust design problem with uncertain Mach number is solved using the proposed approximate statistics evaluation.

The proposed approach has been found particularly effective to estimate statistics for a reasonnable computational cost and drive a shape optimization procedure to a robust wing design.

Acknowledgements

The author gratefully acknowledge the scientific commitee of IDRIS (project 72906) and CINES (project sop2703) for the attribution of CPU time.

References

[1] Guide for the verification and validation of Computational Fluid Dynamics simulation. AIAA guide G-077-1998, 1998.

[2] Andreoli, M., Janka, A., and Désidéri, J.-A. Free-form deformation parameterization for multilevel 3D shape optimization in aerodynamics. INRIA Research Report 5019, November 2003.

[3] Bandemer, H. *Mathematics of uncertainty.* Springer-Verlag, 2006.

[4] Baysal, O., and Burgreen, G. W. Three-dimensional aerodynamic shape optimization using discrete sensitivity analysis. *AIAA Journal 34*, 9 (1996), 1761–1770.

[5] Beux, F., and Dervieux, A. A hierarchical approach for shape optimization. Tech. Rep. 1868, Rapport de Recherche INRIA, 1993.

[6] Buhmann, M. Radial basis functions. *Acta Numerica 9* (2000), 1–38.

[7] Chen, P., and Huang, C. An inverse hull design problem in optimizing the desired wake of a ship. *Journal of Ship Research 46*, 2 (June 2002), 138–147.

[8] Clerc, M., and Kennedy, J. The particle swarm - explosion, stability, and convergence in a multidimensional complex space. *IEEE Transactions on Evolutionary Computation 6*, 1 (February 2002), 58–73.

[9] Courty, F., Leservoisier, D., George, P.-L., and Dervieux, A. Continuous metrics and mesh adaptation. *Appl. Numer. Math. 56*, 2 (2006), 117–145.

[10] Cravero, C., and Satta, A. A hierarchical optimization approach for automatic turbomachinery blade design. AIAA paper 2001-3044, 2001.

[11] Duvigneau, R. Adaptive parameterization using free-form deformation for aerodynamic shape optimization. Research Report 5949, INRIA, 07 2006.

[12] Duvigneau, R., Chaigne, B., and Désidéri, J.-A. Multi-level parameterization for shape optimization in aerodynamics and electromagnetics using a particle swarm optimization algorithm. Research Report 6003, INRIA, 10 2006.

[13] Duvigneau, R., and Pelletier, D. A sensitivity equation method for fast evaluation of nearby flows and uncertainty analysis for shape parameters. *Int. J. of Computational Fluid Dynamics 20*, 7 (August 2006), 497–512.

[14] Duvigneau, R., Pelletier, D., and Borggaard, J. An improved continuous sensitivity equation method for optimal shape design in mixed convection. *Numerical Heat Transfer part B : Fundamentals 50*, 1 (July 2006), 1–24.

[15] Duvigneau, R., Visonneau, M., and Deng, G. On the role played by turbulence closures for hull shape optimization at model and full scale. *Journal of Marine Science and Technology 8*, 1 (June 2003).

[16] Elliott, J., and Peraire, J. Practical 3d aerodynamic design and optimization using unstructured grids. *AIAA Journal 35*, 9 (1997), 1479–1485.

[17] Elliott, J., and Peraire, J. Contrained multipoint shape optimization for complex 3D configurations. *Aeronautical Journal 102*, 1017 (1998), 365–376.

[18] Farin, G. *Curves and Surfaces for Computer-Aided Geometric Design*. Academic Press, 1989.

[19] Fourie, P., and Groenwold, A. The particle swarm optimization algorithm in size and shape optimization. *Structural and Multidisciplinary Optimization 23*, 4 (May 2002), 259–267.

[20] Garzon, V., and Darmofal, D. Using Computational Fluid Dynamics in probabilistic engineering design. In *15th AIAA Computational Fluid Dynamics Conference, Anaheim, USA* (June 2001). AIAA paper 2001–2526.

[21] Godfrey, A. G., and Cliff, E. M. Sensitivity equations for turbulent flows. In *39th AIAA Aerospace Sciences Meeting and Exhibit* (Reno, NV, Jan. 2001). AIAA Paper 2001-1060.

[22] Hay, A., and Visonneau, M. Error estimation using the error transport equation for finite-volume methods and arbitrary meshes. *International Journal of Computational Fluid Dynamics 20*, 7 (August 2006), 463–479.

[23] Huyse, L. Free-form airfoil shape optimization under uncertainty using maximum expected value and second order second moment strategies. Tech. Rep. 2001–18, ICASE, June 2001.

[24] Huyse, L., and Lewis, R. Aerodynamic shape optimization of two-dimensional airfoils under uncertain conditions. Tech. Rep. 2001–1, ICASE, January 2001.

[25] Ilinca, F., and Pelletier, D. Positivity preservation and adaptive solution for the $k-\epsilon$ model of turbulence. *AIAA Journal 36*, 1 (1998), 44–51.

[26] Jameson, A., Martinelli, L., and Pierce, N. A. Optimum aerodynamic design using the Navier-Stokes equation. *Theorical and Computational Fluid Dynamics 10* (1998), 213–237.

[27] Jin, R., Du, X., and Chen, W. The use of metamodeling techniques for optimization under uncertainty. In *ASME Design Engineering Technical Conferences, September 9-11, Pittsburgh, USA* (2001).

[28] Kennedy, J., and Eberhart, R. Particle swarm optimization. In *1995 IEEE International Conference on neural networks, Perth, Australia* (1995).

[29] Li, W., Huyse, L., and Padula, S. Robust airfoil optimization to achieve consistent drag reduction over a Mach range. Tech. Rep. 2001–22, ICASE, August 2001.

[30] Michalewics, Z. *Genetic algorithms + data structures = evolutionary programs*. AI series. Springer-Verlag, New York, 1992.

[31] Mohammadi, B., and Pironneau, O. Mesh adaptation and automatic differentiation in a cad-free framework for optimal shape. *International Journal for Numerical Methods in Engineering 30*, 2 (May 1999), 127–136.

[32] Nakayama, H., Arakawa, M., and Sasaki, R. A computational intelligence approach to optimization with unknown objective functions. In *ICANN 2001 : international conference on artificial neural networks, Vienna , Austria* (2001), pp. 73–80.

[33] Nemec, M., and Zingg, D. Multipoint and multiobjective aerodynamic shape optimization. In *9th AIAA/ISSMO Symposium on Multidisciplinary Analysis and Optimization, Atlanta, USA* (September 2002).

[34] Nielsen, E. J., and Anderson, W. K. Aerodynamic design optimization on unstructured meshes using the Navier-Stockes equations. *AIAA Journal 37*, 11 (1999), 1411–1419.

[35] Oberkampf, W., and Blottner, F. Issues in Computational Fluid Dynamics code verification and validation. *AIAA Journal 36* (1998), 687–695.

[36] Powell, M. Radial basis function methods for interpolation to functions of many variables. In *Fifth hellenic-European conference on Computer Mathematics and its applications* (2001).

[37] Putko, M., Newman, P., Taylor, A., and Green, L. Approach for uncertainty propagation and robust design in cfd using sensitivity derivatives. In *15th AIAA Computational Fluid Dynamics Conference* (Anaheim, CA, June 2001). AIAA Paper 2001-2528.

[38] Roache, P. J. *Verification and Validation in Computational Science and Engineering.* Hermosa publishers, Albuquerque, NM, 1998.

[39] Sederberg, T., and Parry, S. Free-from deformation of solid geometric models. *Computer Graphics 20*, 4 (1986), 151–160.

[40] Shi, Y., and Eberhart, R. A modified particle swarm optimizer. In *International Conference on Evolutionary Computation* (1998), pp. 69–73.

[41] Turgeon, É., Pelletier, D., and Borggaard, J. Application of a sensitivity equation method to the $k-\epsilon$ model of turbulence. In *15th AIAA Computational Fluid Dynamics Conference* (Anaheim, CA, Jun. 2001). AIAA Paper 2001-2534.

[42] Turgeon, É., Pelletier, D., and Borggaard, J. A general continuous sensitivity equation formulation for the $k-\epsilon$ model of turbulence. In *31st AIAA Fluid Dynamics Conference and Exhibit* (Anaheim, CA, Jun. 2001). AIAA Paper 2001-3000.

[43] Turgeon, É., Pelletier, D., and Borggaard, J. Sensitivity and uncertainty analysis for variable property flows. In *39th AIAA Aerospace Sciences Meeting and Exhibit* (Reno, NV, Jan. 2001). AIAA Paper 2001-0139.

[44] Venditti, D., and Darmofal, D. Anisotropic grid adaptation for functional outputs: application to two-dimensional viscous flows. *Journal of Computational Physics 187*, 1 (Mai 2003), 22–46.

[45] Venter, G., and Sobieszczanski-Sobieski, J. Particle swarm optimization. *AIAA Journal 41*, 8 (August 2003), 1583–1589.

[46] Walter, R., and Huyse, L. Uncertainty analysis for fluid mechanics with applications. Tech. Rep. 2002–1, ICASE, February 2002.

[47] Zingg, D., and Elias, S. Aerodynamic optimization under a range of operating conditions. *AIAA Journal 44*, 11 (November 2006), 2787–2791.

Unité de recherche INRIA Sophia Antipolis
2004, route des Lucioles - BP 93 - 06902 Sophia Antipolis Cedex (France)

Unité de recherche INRIA Futurs : Parc Club Orsay Université - ZAC des Vignes
4, rue Jacques Monod - 91893 ORSAY Cedex (France)
Unité de recherche INRIA Lorraine : LORIA, Technopôle de Nancy-Brabois - Campus scientifique
615, rue du Jardin Botanique - BP 101 - 54602 Villers-lès-Nancy Cedex (France)
Unité de recherche INRIA Rennes : IRISA, Campus universitaire de Beaulieu - 35042 Rennes Cedex (France)
Unité de recherche INRIA Rhône-Alpes : 655, avenue de l'Europe - 38334 Montbonnot Saint-Ismier (France)
Unité de recherche INRIA Rocquencourt : Domaine de Voluceau - Rocquencourt - BP 105 - 78153 Le Chesnay Cedex (France)

Éditeur
INRIA - Domaine de Voluceau - Rocquencourt, BP 105 - 78153 Le Chesnay Cedex (France)
http://www.inria.fr
ISSN 0249-6399